Helical Inclusion Complexes of Amylose with Aromatic Compounds: Crystallographic Evidence for New V-Type Allomorphs

Cong Anh Khanh Le, Yu Ogawa, Florent Grimaud, Yoshiharu Nishiyama, I. Morfin, Gabrielle Potocki-Veronese, Luc Choisnard, Denis Wouessidjewe, Jean-Luc Putaux

Helical Inclusion Complexes of Amylose with Aromatic Compounds: Crystallographic Evidence for New V-type Allomorphs

Cong Anh Khanh Le[1], Yu Ogawa[1], Florent Grimaud[2], Yoshiharu Nishiyama[1], Isabelle Morfin[3], Gabrielle Potocki-Veronese[2], Luc Choisnard[4], Denis Wouessidjewe[4], Jean-Luc Putaux[1,]*

[1] Univ. Grenoble Alpes, CNRS, CERMAV, F-38000 Grenoble, France

[2] TBI, CNRS, INRAE, INSAT, Université de Toulouse, F-31400 Toulouse, France

[3] Univ. Grenoble Alpes, CNRS, LiPhy, F-38000 Grenoble, France

[4] Univ. Grenoble Alpes, CNRS, DPM, F-38000 Grenoble, France

*corresponding author: jean-luc.putaux@cermav.cnrs.fr

Published in: **Crystal Growth & Design** *22* (2022), 7079-7089

DOI: 10.1021/acs.cgd.2c00771

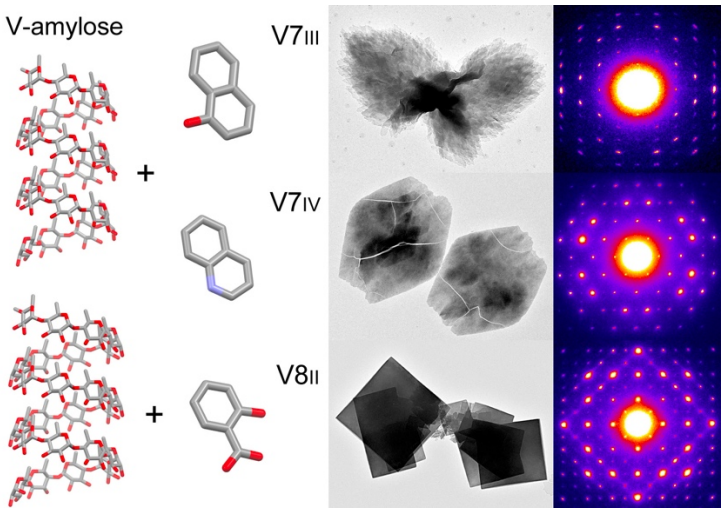

ABSTRACT

Amylose, a mostly linear homopolymer of glucosyl units extracted from native starch granules, can form a large variety of so-called V-type host-guest complexes when cocrystallized with small hydrophobic molecules. Several allomorphs are known that contain 6-, 7- or 8-fold amylose single helices, the guest molecules being located in the helices, in-between, or both. The present report describes the crystal structure of model lamellar inclusion complexes prepared by crystallizing amylose from dilute aqueous solutions in the presence of three aromatic compounds, namely napth-1-ol, salicylic acid, and quinoline. By adequately selecting the crystallization conditions (amylose chain length, mixing and crystallization temperatures), each guest induced two allomorphs, characterized by transmission electron microscopy, X-ray and electron diffraction, and ^{13}C CP/MAS solid-state NMR spectroscopy data. The three guests induced the formation of the tetragonal $V8_{II}$ allomorph, based on 8-fold amylose single helices, whereas three other allomorphs were identified for the first time: $V7_{III}$ (with napht-1-ol), $V7_{IV}$ (with quinoline), both based on orthorhombic unit cells containing 7-fold helices, and the monoclinic $V8_{III}$ (with salicylic acid). The results widen the family of known V-amylose allomorphs that may occur when starch is processed in the presence of various ingredients and additives.

1. INTRODUCTION

Amylose is a mostly linear homopolymer of glucosyl units and one constituent of native starch granules.[1] Linear amylose-like polymers can also be biosynthesized *in vitro* by amylose synthases such as amylosucrase[2] or starch phosphorylase.[3] A large variety of host-guest cocrystals can be prepared by crystallizing amylose in the presence of small hydrophobic molecules.[4–7] Pure amylose forms 6-fold double-helices that assemble into two possible allomorphs, namely the monoclinic A-type and the hexagonal B-type. However, in the presence of a ligand, amylose adopts a single helical conformation.[1] The resulting inclusion compounds are known under the generic name of "V-amylose". In these crystals, the guest molecules can be entrapped in the hydrophobic cavity of the amylose helices and/or between them.[6,8] This property can be used, for instance, to develop ingredients for functional foods or encapsulate weakly soluble compounds and subsequently release them under controlled conditions.[9–16] Determining the crystal structure of the complexes is thus crucial to understand such host-guest interaction.

When crystallized from dilute aqueous solutions, amylose yields micrometer-sized but 8-10 nm-thick lamellar single crystals.[17–19] If the chain length is much longer than the typical thickness of a lamella, amylose folds at the surface like flexible synthetic polymers.[20,21] The chain-folding is facilitated by a low-energy "band-flip" between two adjacent glucosyl moieties that enables an easy reversal of the molecular trajectory.[22] The morphology and structure of the crystals depends on the type of guest as well as crystallization parameters like amylose and guest concentrations and temperature.[1]

Several V-amylose allomorphs have been reported that can be distinguished by their X-ray diffraction (XRD) pattern recorded from powders,[23,24] mats of sedimented crystals[25–27] or stretched films.[28–29] Transmission electron microscopy (TEM) has been a technique of choice to determine the habit of V-amylose lamellar crystals and simultaneously collect electron diffraction (ED) data. When the electron beam was oriented perpendicular to the crystal plane, *i.e.* parallel to the helical axis, the dimensions and symmetry of the unit cell was determined and helicities and helix packings proposed.[17–19,24,30,31] In some cases, high-order ED data were also collected from crystals tilted about selected crystallographic axes.[17,18,30,32] Considering the high beam sensitivity of V-amylose crystals and the possibility that included guest molecules can be lost by evaporation in the microscope vacuum, care was taken to preserve the crystal structure during data collection. Therefore, the specimens were quench-frozen in liquid nitrogen before their insertion in the microscope and observed at cryo temperature under low dose illumination conditions.[30,31]

So far, all proposed molecular models of V-amylose crystals have been based on antiparallel packings of left-handed single helices with 6, 7 or 8 glucosyl units per pitch.[17,33–35] Since the helical pitch is about 0.80 nm regardless the number of glucosyl residues per turn, the diameter of the helices increases with increasing helicity, allowing to accommodate bulkier molecules. Each allomorph was named "Vx_y", where "x" is an Arabic number that represents the helicity of amylose (6, 7 or 8) and subscript "y" is a Roman number (I, II, III, etc.). The $V6_I$ allomorph, also often referred to as V_h, has been reported for crystals prepared with primary alcohols[17,29,36] linear fatty acids[24,37] and some aliphatic diols.[31] The crystals are hexagonal and the helices are close-packed into a hexagonal[17] or pseudo-hexagonal[29] unit cell. The guest is partly or totally included inside the helix cavity. The $V6_{II}$ structure has been proposed for complexes with butan-1-ol and pentan-1-ol,[30,38] as well as some fatty acids and diols.[24,31] In this structure, the 6-fold helices contain guest molecules but are arranged in such a way that the interhelical space is large enough to accommodate ligands.[38] A $V6_{III}$ structure has previously been inferred for $V_{propan\text{-}2\text{-}ol}$ complexes[23] but it was later demonstrated that the complex indeed contained 7-fold helices.[35] Therefore, the $V6_{III}$ denomination should rather refer to the allomorph obtained by crystallizing amylose with DMSO[39] or glycerol[40] into square crystals with an orthorhombic unit cell and guests possibly located inside and between helices.

Hexagonal $V_{borneol}$ and $V_{camphor}$ crystals were described as containing close-packed 7-fold helices and, by analogy with the $V6_I$ / V_h structure, the allomorph was referred to as $V7_I$.[41] A $V7_{II}$ allomorph was characterized for complexes with propan-2-ol,[26,35] thymol, carvacrol,[42] menthone, fenchone, linalool,[43] and terpineol,[44] and it has recently been shown that $V_{ibuprofen}$,[33] and $V_{pentadecylphenol}$[13] were isomorphous complexes. All lamellar crystals are rectangular and yield similar base-plane ED patterns with only minor variations in spot intensities. The guest would be included in the helices and in-between. Eight-fold helices were reported to occur in a small number of complexes prepared with bulkier guests, namely naphth-1ol,[27,32,42] quinoline,[42,44] and salicylic acid.[45] Square crystals were observed in the case of $V_{napht\text{-}1\text{-}ol}$ and $V_{quinoline}$, the helices being organized into a tetragonal unit cell with ligands located inside them and in-between.[32,44] Since the $V8_I$ name has already been proposed for the close-packing of 8-fold helices in complexes with salicylic acid,[46,47] we will refer to the tetragonal structure as $V8_{II}$ in the following.

In addition, drying the crystalline complexes under vacuum or washing them in methanol can also induce dehydration and/or desolvation effects that result in structural transitions. In particular, close-packed structures referred to as $V6_a$, $V7_a$, or $V8_a$ can form with unit cells slightly smaller than those of the $V6_I$, $V7_I$, or $V8_I$ counterparts.[31,41]

The general features of the main allomorphs described above according to the morphology of lamellar single crystals, diffraction data and assumed helicity, have been defined in the 1960's and 1970's.[25–27] Refinements and revisions have been proposed in more recent years[30,32,35] and it has been shown that polymorphism, in terms of helicity and molecular packing, exists for given complexing agents.[24,31] However, no new V-type allomorph has been recently observed and described. We have previously explored the polymorphism of V-amylose cocrystallized with linear saturated fatty acids[24] and aliphatic diols.[31] In these cases, $V6_I$, $V6_{II}$, $V7_I$ and $V7_{II}$ allomorphs were obtained with the same ligand by varying the crystallization parameters (amylose chain length, solvent composition, incubation temperature). In the present work, using complementary imaging, diffraction, and spectroscopy techniques, we have characterized the morphology, helicity, and crystal structure of highly crystalline lamellar V-amylose complexes prepared with bulkier aromatic compounds, namely napht-1-ol, salicylic acid and quinoline, known to induce the formation of larger 8-fold amylose helices.[27,32,44,45] Based on our highly resolved structural data, we have shown that these guests also promoted the crystallization of different V-amylose allomorphs, three of which were identified and described for the first time.

2. EXPERIMENTAL SECTION

2.1. Materials

Native potato amylose purchased from Sigma-Aldrich was purified as previously described.[24] Its chain length distribution was analyzed by size exclusion chromatography (SEC) with multi-angle laser light scattering (MALLS) from a solution of amylose dissolved in lithium chloride / N,N-dimethyl acetamide (LiCl/DMAc) and the distribution of degree of polymerization (DP) of each fraction was determined by high-performance anion-exchange chromatography with pulsed amperometric detection (HPAEC-PAD).[31] With a weight-average DP ($\overline{DP_w}$) of 2514, the fraction of native amylose will be referred to as DP2500 in the following. Using the protocol described by Potocki-Veronese et al.,[48] a linear amylose-like polymer was enzymatically synthesized *in vitro* from sucrose by the amylosucrase from *Neisseria polysaccharea* (with $\overline{DP_w}$ = 86), and subsequently fractionated by preparative SEC.[31] Fractions with $\overline{DP_w}$ = 60, 80 and 130 (referred to as DP60, DP80 and DP130) were selected for crystallization (Supporting information Figure S1). An amylose fraction with $\overline{DP_w}$ = 192 (referred to as DP200), synthesized *in vitro* by a glycoside-phosphorylase, was purchased from Shoko Co. Ltd (Japan). The characteristics of all fractions are summarized in **Table 1**. Napht-1-ol (napthalen-1-ol), salicylic acid (2-hydroxybenzoic acid) and quinoline (1-benzopyridine) were purchased from Sigma-Aldrich (**Scheme 1**). They will be referred to as NAP1, SAL and QN, respectively, in the following.

Table 1. Molecular characteristics of the fractions used in this study. $\overline{DP_w}$ is the weight-average degree of polymerization. $\overline{M_w}$ and $\overline{M_n}$ are the weight- and number-average molecular weights, respectively.

Fraction	DP60 [a]	DP80 [a]	DP130 [a]	DP200 [b]	DP2500 [c]
$\overline{DP_w}$	60	80	130	192	2514
$\overline{M_w}$ (g mol^{-1})	9738	12816	21078	31200 [d]	407268
$\frac{\overline{M_w}}{\overline{M_n}}$	1.05	1.07	1.07	1.01 [d]	2.70

[a] synthesized *in vitro* by the amylosucrase from *N. polysaccharea*.[48]
[b] synthesized *in vitro* by a glucoside-phosphorylase.[3]
[c] native potato amylose.[33.] [d] values provided by the manufacturer.

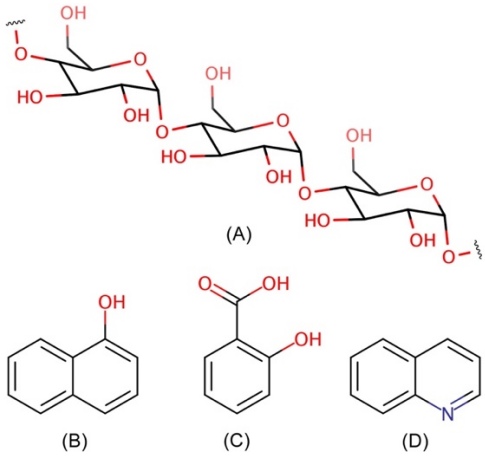

Scheme 1. Chemical structure of amylose (A), napht-1-ol (B), salicylic acid (C) and quinoline (D), drawn with MarvinSketch.[49]

2.2. Crystallization protocols

Aqueous amylose dispersions (10 mL at 0.1 wt%) of DP60, DP80, DP130, DP200, and DP2500 fractions were submitted to nitrogen bubbling for 20 min, then autoclaved in an oil bath at 160 °C for 30 min and cooled down to 60–90 °C before the addition of the complexing agent. For each of the three ligands, specific preparation conditions were used, which are described in the following.

2.2.1. Napht-1ol (NAP1)

An excess amount of NAP1 powder (10 mg) was added to the amylose solutions at 60, 70 or 90 °C. The mixtures were kept for 1 h at this temperature, then allowed to cool down to room temperature. The crystallization gradually occurred upon cooling and was complete after one day. The crystals were washed by successive sedimentation in water saturated with NAP1, and stored in this mother liquor in a tightly closed vial, in the dark, at room temperature.

2.2.2. Salicylic acid (SAL)

An excess amount of SAL powder (10 mg) was added to the amylose solutions at 75 °C and the mixture was incubated for 1 week at 25, 40, 60 or 75 °C. The crystals were washed by successive sedimentation in water saturated with SAL and kept in this mother liquor at room temperature.

2.2.3. Quinoline (QN)

An excess amount of preheated liquid QN (0.25-3 mL) and 10-30 vol% DMSO were added to the amylose solutions at 75 °C. The mixtures were incubated for 2 weeks at 25, 40, 60 or 75 °C. Since QN is denser than water (ρ = 1.093 g cm^{-3}), the excess lay at the bottom of the vial. The crystals slowly sedimented on top of the excess QN which was then removed by pipetting. The crystals were washed three times by sedimentation in water saturated with QN and kept in this mother liquor at room temperature.

2.3. X-ray diffraction (XRD)

The crystal suspensions were centrifuged and the wet pellets were deposited on a 7-µm nylon bolting cloth, desorbed over a salt-saturated aqueous solution yielding a 95% relative humidity (R.H.). Strips of the resulting films were inserted into 1 mm (outer diameter) glass capillaries which were immediately flame-sealed.

2.3.1. Laboratory analyses

The specimens were X-rayed in transmission with a Ni-filtered CuKα radiation (λ = 0.1542 nm) in a Warhus vacuum camera mounted on a Philips PW3830 generator operating at 30 kV and 20 mA. Two-dimensional diagrams were recorded on Fujifilm image plates during 2 h and read with a Fujifilm BAS 1800-II bioimaging analyzer. Diffraction profiles were calculated by radially averaging the ring patterns. The data were calibrated using a calcite ($CaCO_3$) standard and the unit cell parameters were refined with the CelRef module of the LMGP package.[50]

2.3.2. Synchrotron X-ray diffraction analyses

The WOS silicon pixel detector (imXPAD, France) was placed at a distance of 0.14 m from the sample to cover a *q*-range from 0.6 to 4.0 $Å^{-1}$. Scattering patterns were collected during 50-s exposures, with a beam energy of 18 keV (λ = 0.0689 nm). Diffraction profiles were calculated by radially averaging the ring patterns. The data were calibrated using a chromium oxide (Cr_2O_3) standard and the unit cell parameters were refined with the CelRef module of the LMGP package.[50]

2.4. Transmission electron microscopy (TEM) and electron diffraction (ED)

Drops of dilute crystal suspensions were deposited onto glow-discharged carbon-coated grids and allowed to dry. The specimens were observed under low dose illumination with a Thermo

Scientific Philips CM200 'Cryo' microscope operating at 200 kV. For electron diffraction, the specimens were mounted in a Gatan 626 holder, quench-frozen in liquid nitrogen, introduced in the microscope and observed a low temperature (-180 °C). Images and ED patterns were recorded with a TVIPS TemCam F216 digital camera. In the following, "base-plane ED patterns" will refer to patterns recorded along the [001] *c*-axis of the crystal structure, *i.e.*, perpendicular to the *(a,b)* plane of the lamellae and parallel to the axis of the amylose helices. The diffraction patterns were calibrated using a gold-coated carbon film standard and the unit cell parameters were refined using a least-squares regression method.

2.5. ^{13}C CP/MAS NMR spectroscopy

Crystal suspensions were centrifuged. The excess liquid was blotted off and the hydrated pellets were packed into zirconia rotors. Solid-state ^{13}C NMR spectra were recorded with a Bruker Avance III 400 MHz spectrometer (^{13}C frequency of 100.6 MHz) using magic angle spinning (MAS) and cross-polarization (CP). The spinning speed was set at 12 kHz, with a sweep width of 29761 Hz and a recycle delay of 2 s. Each spectrum was averaged over about 6000 scans. The ^{13}C chemical shifts were calibrated with respect to the resonance of the glycine carboxyl group (176.03 ppm).

2.6. Molecular modeling

Stereoregular left-handed 7- and 8-fold amylose helices with a pitch of 0.80 nm were generated from an α-D-glucosyl residue in the $^4C_1$ chair shape as described elsewhere[35] and energy-minimized using the Universal Force Field[51] in the Forcite module of Biovia Materials Studio 5.5.[52] The helices were introduced into the unit cell with parameters and space group determined from the ED and XRD data. All models were visualized and drawn using the Mercury software.[53]

3. RESULTS AND DISCUSSION

3.1. Morphology and structure of individual allomorphs

For each of the three tested guests, crystalline complexes corresponding to two different allomorphs were obtained, depending on the formulation or crystallization parameters (amylose DP, solvent, mixing or incubation temperature). These allomorphs were readily distinguished by the morphology of the lamellar crystals observed by TEM and by the crystal structure determined from base-plane ED and XRD patterns.

3.1.1. The tetragonal V8$_{II}$ form

The three guests induced the formation of square crystals (**Figure 1A,D,G**) exhibiting similar base-plane ED (**Figure 1B,E,H**) and XRD (**Figures 1C,F,I** and **S2A,B**) patterns. Some variation

in diffraction intensities was observed (**Figure 4**), likely due to differences in crystal thickness, crystallinity degree of the complex or preferential orientation of the lamellae in the solvated specimens prepared for XRD analysis. In particular, a reflection at q = 3.8 nm^{-1} can be seen in the XRD pattern (**Figure 1C,F,I**) and profile (**Figure S3A-C**) of V_{SAL} crystals that is absent from those of V_{NAP1} and V_{QN} (**Figure S4**). The V_{QN} complex was less crystalline, with many extinct ED spots, and each reflection exhibited streaks parallel to the main crystallographic layer lines, which suggests the presence of numerous defects such as stacking faults. An XRD ring at a lower angle ($q \approx 0.41$ nm^{-1}) in the V_{QN} XRD pattern (**Figure S4C**) likely corresponds to the average thickness of individual crystals packed upon film formation, *i.e.* 15.3 nm, consistent with the multiple chain-folding of DP2500 amylose. No such ring was observed for the V_{NAP1} and V_{SAL} specimens, suggesting that the X-ray beam was perpendicular to the crystal mat, hence parallel to the helix axis.

The tetragonal unit cell parameters calculated as an average of the parameters of the three complexes determined from the XRD profiles were $a = b = 2.311 \pm 0.001$ nm and $c = 0.790 \pm 0.001$ nm (**Tables 2**, **S1** and **S2**), in good agreement with the values previously reported from V_{NAP1} complexes.[32] Yamashita and Monobe[27] and Helbert[42] proposed a tetragonal packing of 8-fold helices, which was validated by Cardoso et al. from high-resolution lattice images of lamellar single crystals.[32] A model of The $V8_{II}$ structure with space group is $P4_32_12$ is shown in **Figure 6C**. Helbert calculated a and b unit cell parameters of V_{QN} crystals that were twice as large as those of V_{NAP1} crystals.[42] However, Putaux et al. recorded a V_{QN} ED pattern identical to that of V_{NAP1} crystals and concluded that the parameters were the same,[54] as was confirmed by our present results. Although it has been suggested that 8-fold amylose helices occurred in complexes with salicylic acid[45] and salicylic acid analogues,[46] to our knowledge, it is the first time that the tetragonal allomorph has been unambiguously identified for V_{SAL} from crystallographic data.

3.1.2. The new allomorphs

3.1.2.1. New Allomorph of $V_{napht\text{-}1\text{-}ol}$

The crystals consist of stacks of several lamellae with a rhombohedral habit and an average acute angle of about 64° (Figure 2A,B). The crystals likely developed via epitaxial growth of new lamellae rather than a dislocation-centered spiral growth mechanism. Twinned structures at an angle of about 64° were also often observed (Figure 2C). The average thickness of the lamellae prepared with DP2500 amylose, deduced from the low-angle XRD ring (Figure S5A) was 10.3 nm ($q \approx 0.61$ nm^{-1}). The ED pattern of the crystals shown in Figure 3A can be indexed along a rectangular unit cell with $a = 1.66 \pm 0.01$ nm and $b = 2.50 \pm 0.01$ nm, in agreement with the values calculated from the XRD profile ($a = 1.663 \pm 0.001$ nm, $b = 2.518 \pm 0.001$ nm and $c = 0.856 \pm 0.001$ nm) (**Tables 2**,

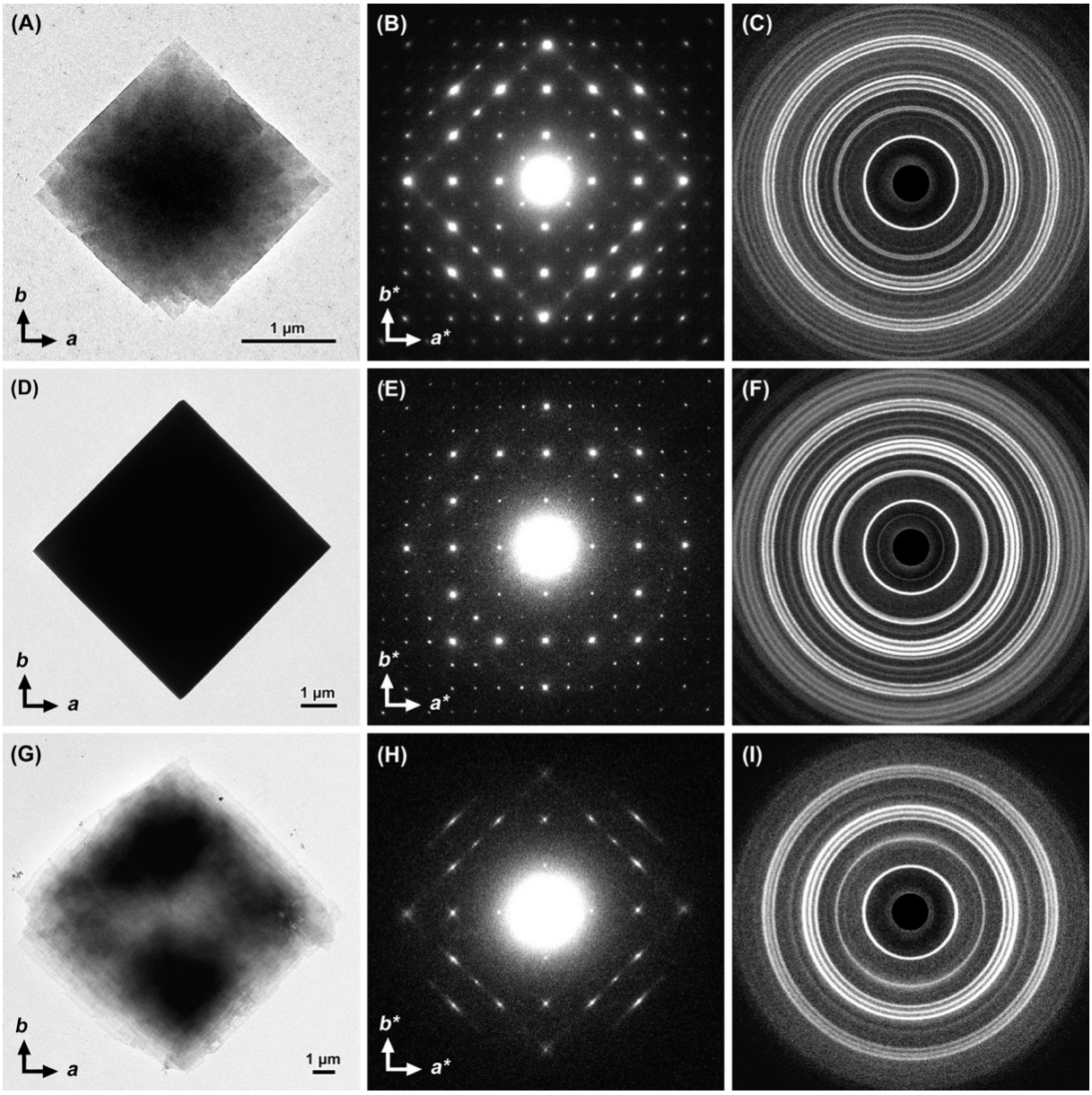

Figure 1. TEM images (A,D,G), base-plane ED patterns (B,E,H) and XRD diagrams (C,F,I) of V-amylose crystals corresponding to the $V8_{II}$ allomorph: (A–C) V_{NAP1} (DP130, mixing at 75 °C, no incubation time); (D–F) V_{SAL} (DP60, incubation at 40 °C); (G–I) V_{QN} (DP2500, incubation at 40 °C, 30 vol% DMSO). The ED patterns were recorded at low temperature from frozen-solvated crystals. For clarity, the XRD patterns are those recorded with the laboratory set-up. The composite patterns collected at ESRF are shown in Supporting Information **Figure S5**.

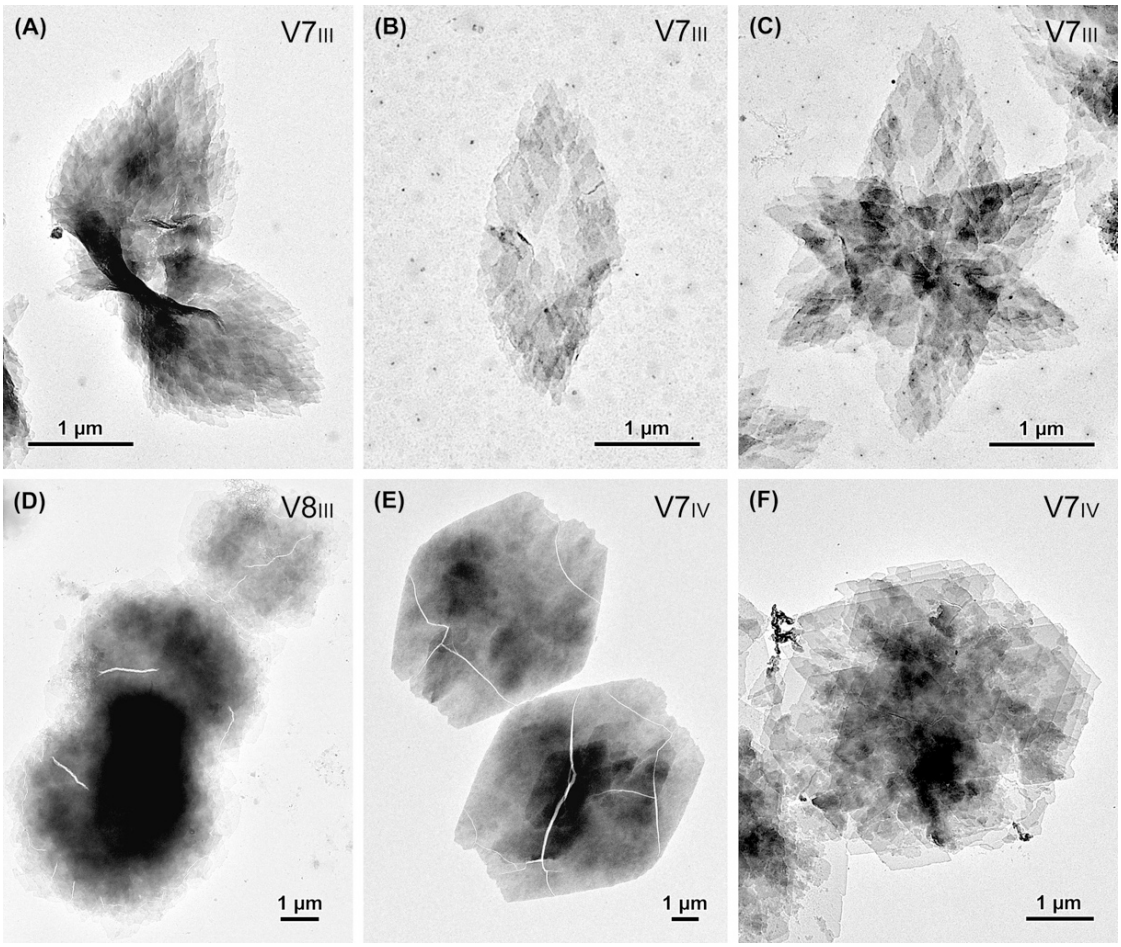

Figure 2. TEM images showing the typical morphology of lamellar crystal assemblies of V-type complexes corresponding to new allomorphs: (A–C) V_{NAP1} ($V7_{III}$ – DP2500, mixing at 75 °C); (D) V_{SAL} ($V8_{III}$ – DP200, incubation at 60 °C); (E) V_{QN} ($V7_{IV}$ – DP80, no DMSO, incubation at 25 °C); (F) V_{QN} ($V7_{IV}$ – DP130, no DMSO, incubation at 25 °C).

S1 and **S3**). The *c*-parameter is slightly larger than that of other known V-type allomorphs that generally varies between 0.79and 0.83 nm.[17,18,32,40] In addition, only *h*00, 0*k*0, and 00*l* reflections with even indices were observed, suggesting that the unit cell is orthorhombic with space group $P2_12_12_1$. The *a*-parameter corresponds to the center-to-center distance between neighboring 8-fold helices in the $V8_{II}$ unit cell described in section 3.1.1 and **Figure 6C**. It is thus the external diameter of 8-fold helices. A pseudo-hexagonal orthorhombic packing would have $b = a\sqrt{3} = 2.880$ nm that is 14% larger than the experimental 2.518 nm. Therefore, the helices would be significantly compressed along the *b*-axis, generating unlikely molecular contacts. This new V_{NAP1} allomorph would rather contain 7-fold helices (1.50 nm in diameter[26,35,41,55]) in a compact arrangement or 6-fold helices (1.37 nm in diameter[17,25]) with a looser packing. **Figure 6A** shows a possible close packing of 7-fold helices in the unit cell with space group $P2_12_12_1$. The unit cell contains two amylose

helices and NAP1 guests can be located inside the helices but not in-between. From this geometrical analysis only, it is not possible to unambiguously conclude whether the complexes contain 6- or 7-fold helices. However, additional information on the helicity will be provided by the solid-state NMR data presented in **section 3.2**.

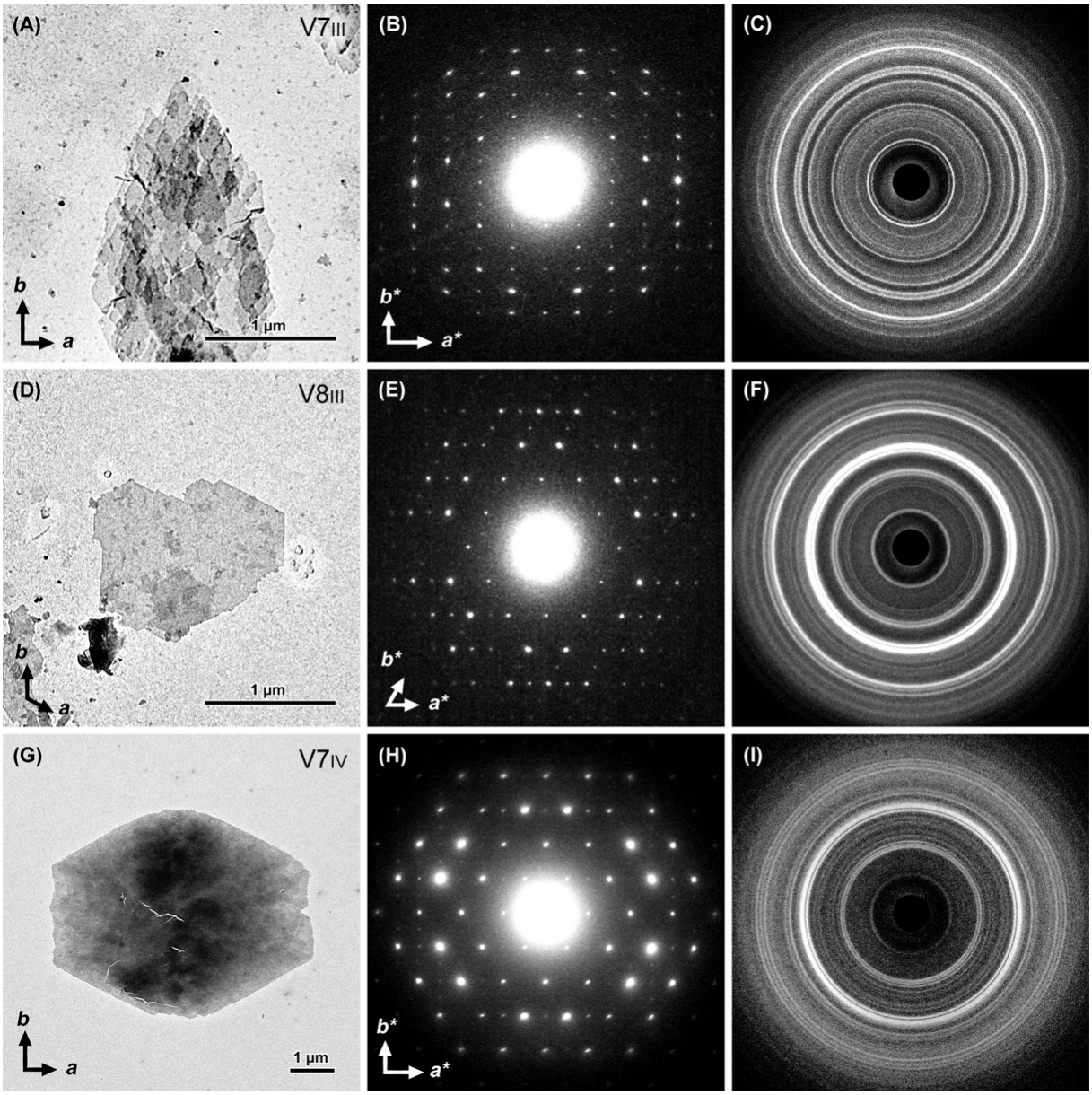

Figure 3. TEM images (A,D,G), base-plane ED patterns (B,E,H) and XRD diagrams (C,F,I) of V-amylose crystals corresponding to new allomorphs: (A–C) V_{NAP1} ($V7_{III}$ – DP2500, mixing at 75 °C); (D–F) V_{SAL} ($V8_{III}$ – DP200, incubation at 60 °C); (G–I) V_{QN} ($V7_{IV}$ – DP80, no DMSO, incubation at 25 °C). The ED patterns were recorded at low temperature from frozen-solvated crystals. For clarity, the XRD patterns are those recorded with the laboratory set-up. The composite patterns collected at ESRF are shown in Supporting Information **Figure S5**.

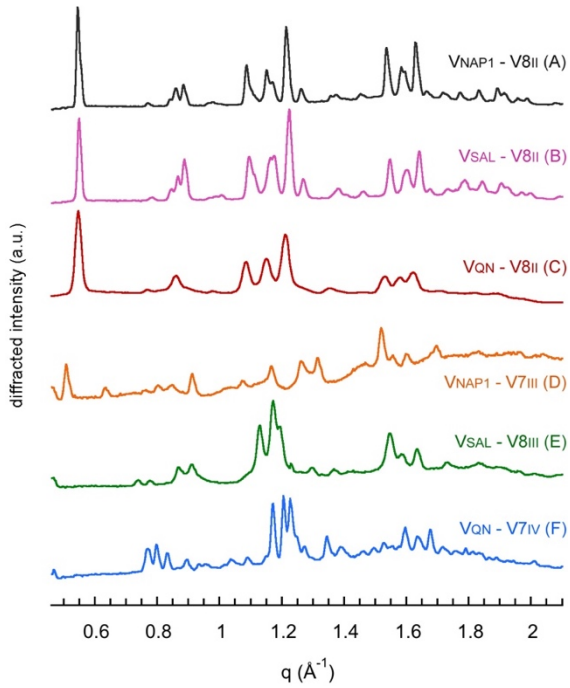

Figure 4. XRD profiles of the solvated V-type complexes resulting from the cocrystallization of amylose with napht-1ol (NAP1), salicylic acid (SAL) and quinoline (QN) calculated as radial averages of the 2D patterns shown in Supporting Information **Figure S5**: (A) V_{NAP1} ($V8_{II}$ – DP80, mixing at 60 °C for 30 min), (B) V_{SAL} ($V8_{II}$ – DP60, incubation at 25 °C), (C) V_{QN} ($V8_{II}$ – DP2500, 30 vol% DMSO, incubation at 40 °C), (D) V_{NAP1} ($V7_{III}$ – DP2500, mixing at 75 °C), (E) V_{SAL} ($V8_{III}$ – DP2500, incubation at 60 °C), (F) V_{QN} ($V7_{IV}$ – DP80, no DMSO, incubation at 25 °C). Profiles A, B and D– E were calculated from ESRF data, while profile C is from the laboratory data.

3.1.2.2. New allomorph of $V_{salicylic\ acid}$

Figures 2D and **3D** show TEM images of typical crystals of the new form of V_{SAL}. The crystals consist of stacks of many lamellae with both epitaxial and dislocation-centered spiral growths. The shape of individual lamellae cannot be defined with precision. The crystals generally exhibit a broadly hexagonal shape that is close to those of V-type complexes with linear fatty acids in the $V6_I$ form,[24] some diols ($V6_I$ form),[31] and (–)-borneol ($V7_I$ form).[41] The average thickness of the lamellae prepared with DP2500 amylose is 12.5 nm ($q \approx 0.50$ nm^{-1}) (**Figure S5B**). A typical base-plane ED pattern recorded from one frozen-solvated lamella of V_{SAL} is shown in Figure 3E. This pattern shows a centrosymmetry ($I_{hkl} = I_{\bar{h}\bar{k}\bar{l}}$) but there is no mirror plane. The base-plane ED pattern can be indexed along a unit cell with parameters $a = 3.21 \pm 0.01$ nm, $b = 3.23 \pm 0.01$ nm, and $\gamma = 116.9 \pm 0.3°$. These parameters agree with those calculated from the XRD profile (Figure 3F, Tables 2, S1 and S2): $a = 3.245 \pm 0.006$ nm, $b = 3.246 \pm 0.005$ nm, $c = 0.793 \pm 0.001$ and $\gamma = 116.62 \pm 0.13°$. Since there is no systematic absence based on the h and k indices, the space group would be $P2$ or $P2_1$. Assuming a close packing, the center-to-center distance of helices would be 1.62 nm consistent with 8-fold helices.[27,32] Therefore, 6-, 7- or 8-fold helices would fit into the

unit cell. A tentative geometrical model with a close packing of 8-fold helices and a $P2_1$ symmetry is shown in Figure 6D. Each monoclinic unit cell contains four amylose helices. Salicylic acid would be located inside the helical cavity but not in-between. Additional details on the helical conformation were given by CP/MAS solid-state NMR (**section 3.2**).

3.1.2.3. New allomorph of $V_{quinoline}$

The crystals of a new form of V_{QN} prepared from the DP80 fraction exhibit a truncated rhombohedral habit with an average obtuse angle of about 116° and consist of several superimposed smaller lamellae in epitaxial orientation (**Figures 2E** and **3G**). The crystals prepared with longer amylose chains, such as those prepared with DP130 amylose (**Figure 2F**), were usually stacks of lamellae with a more or less hexagonal shape that recalls that of V-type complexes with linear fatty acids ($V6_I$ form),[24] some diols ($V6_I$ form),[31] and (–)-borneol ($V7_I$ form).[41] The average lamellar thickness could not be determined since no low-angle ring was detected in the XRD pattern of crystals prepared from DP130 amylose (**Figure S5C**). Typical ED and XRD patterns recorded from frozen-solvated crystals are shown in **Figure 3H** and **3I**, respectively. The ED pattern can be indexed on the basis of a rectangular unit cell with parameters a = 2.67 ± 0.01 nm and b = 3.23 ± 0.01 nm, in agreement with those calculated from XRD data (a = 2.702 ± 0.001 nm, b = 3.291 ± 0.001 nm and c = 0.786 ± 0.001 nm - **Tables 2**, **S1** and **S3**). In addition, the $h00$, $0k0$ and $00l$ reflections are absent when h, k or l is odd, suggesting an orthorhombic unit cell with $P2_12_12_1$ space group. Assuming a compact packing, the helix diameter would be 1.56 nm, which is smaller than the diameter of an 8-fold helix but larger than that of 6- or 7-fold helices. Therefore, the complexes could contain 6- or 7-fold helices. A geometrical model based on the packing of stereoregular 7-fold helices is shown in Figure 6A. Each unit cell contains four amylose helices. Quinoline would only be located inside the helical cavity. Additional details on the helical conformation were given by CP/MAS solid-state NMR (**section 3.2**).

3.2. ^{13}C CP/MAS NMR spectroscopy

Typical ^{13}C CP/MAS NMR spectra of the solvated V-amylose complexes are shown in **Figure 5**. The resolved resonances in the carbohydrate region (55–100 ppm) can be assigned to the carbons of the glucosyl units of the amylose chains. A weak peak at 100.3 ppm was also observed in some spectra, corresponding to the C1 resonance of B-type amylose, likely corresponding to a small fraction of recrystallized uncomplexed amylose.[56,57] Peaks corresponding to traces of excess ligands can be seen in the 110–180 ppm region. In particular, the contributions of the aromatic carbons in the three guests appear in the 123–143 ppm region.

Previous CP/MAS NMR studies of crystalline V-amylose complexes revealed that the C1 chemical shift was correlated with the torsion angle ϕ (O5–C1–O1–C4) around the glucosidic linkages (**Scheme S1**).[56,58,59] It was thus suggested that the position of carbon C1 resonance was characteristic of the number of glucosyl units per turn in the amylose helix.[56,58] In the present study, the helicity of V-amylose in the allomorphs was thus determined based on the position of the C1 peak. The complexes with NAP1, QN and SAL corresponding to square crystals had C1 resonances located at 103.9, 104.4 and 103.9 ppm, respectively (**Figure 5A-C**). Since V_{NAP1} has previously been shown to contain 8-fold helices,[32] we assumed that isomorphous V_{QN} and V_{SAL} did as well. The C1 resonance of the new V_{SAL} allomorph, located at 103.9 ppm, also suggests a V8 helicity (**Figure 5D**). The C1 resonance of the new V_{QN} allomorph is located at 103.5 ppm (**Figure 5E**). This value is close to that of $V_{ibuprofen}$ (103.4 ppm),[33] $V_{propan\text{-}2\text{-}ol}$ (103.3 ppm),[33,58] $V_{menthone}$ and $V_{linalool}$ (103.3–103.4 ppm).[58,60,61] Although these complexes have different crystal structures, they were all assumed to contain V7 helices, which would thus be the case for the new V_{QN} allomorph. The C1 resonance region of the new form of V_{NAP1} is more complex. It is a multiplet with three main peaks located at 98.6, 103.4 and 105.9 ppm (**Figure 5F**). None of these peaks corresponded to those of excess solid NAP1. The splitting of the resonance reflects the presence of inequivalent environments within the material.[56,57] Therefore, we assumed that the single helices in V_{NAP1} were less symmetrical than those in other allomorphs and contained several asymmetric glucose units. However, the strongest C1 signal at 103.4 ppm suggests that the new allomorph of V_{NAP1} contains 7-fold amylose helices. Overall, the helical conformation determined from the C1 resonance is in good agreement with that predicted on the basis of geometrical models of close-packed helices and helix diameter deduced from diffraction data.

3.3. Nomenclature

The analysis of the crystallographic and spectroscopic data allowed identifying three new V-type allomorphs prepared by co-crystallizing amylose with NAP1, SAL and QN, respectively. As a consequence, three new names must be added to the list of already known crystal forms. Using the naming system that was described in the introduction, the new V_{NAP1}, V_{QN} and V_{SAL} allomorphs will be referred to as $V7_{III}$, $V7_{IV}$ and $V8_{III}$, respectively, in the following (**Table 2**). It must be noted that, although it was supported by solid-state NMR data, the helical conformation in $V7_{III}$ and $V7_{IV}$ could not be unambiguously determined from the crystallographic data. The proposed nomenclature thus reflects the present state of knowledge and may be revised in the future after new datasets have been collected.

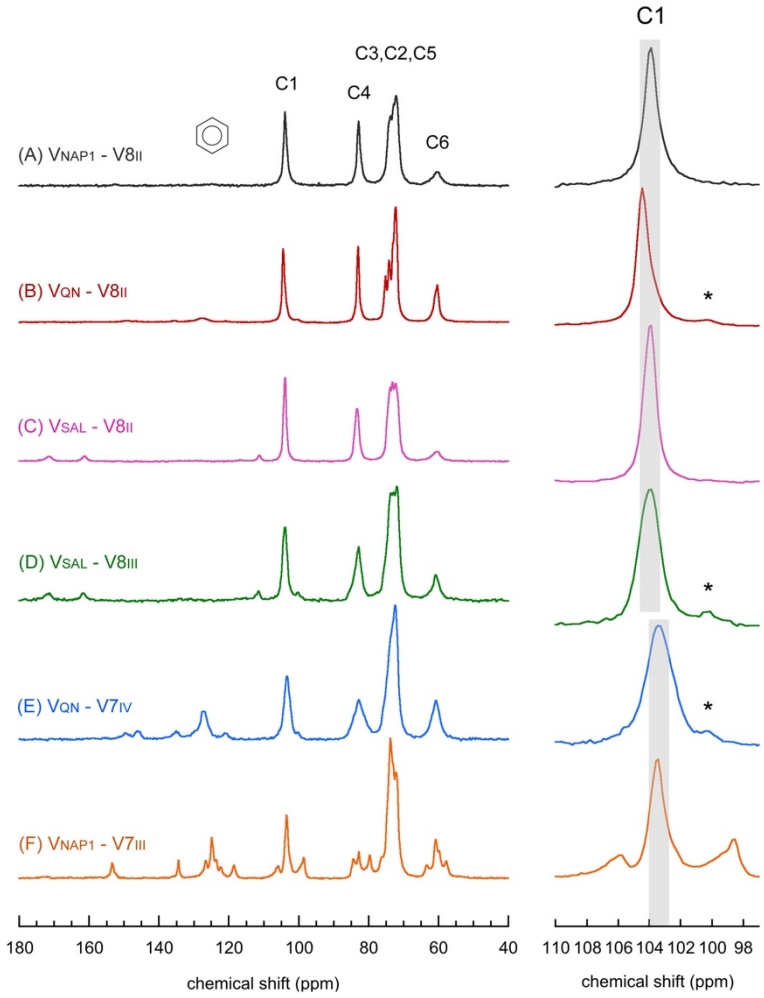

Figure 5. ^{13}C CP/MAS solid-state NMR spectra of the solvated V-type complexes that resulted from the cocrystallization of amylose with napht-1-ol (NAP1), quinoline (QN), and salicylic acid (SAL): (A) V_{NAP1} ($V8_{II}$ – DP80, mixing at 60 °C); (B) V_{QN} ($V8_{II}$ – DP2500, 30 vol% DMSO, incubation at 40 °C); (C) V_{SAL} ($V8_{II}$ – DP60, incubation at 25 °C); (D) V_{SAL} ($V8_{III}$ – DP2500, incubation at 60 °C); (E) V_{QN} ($V7_{IV}$ – DP2500, no DMSO, incubation at 25 °C); (F) V_{NAP1} ($V7_{III}$ – DP2500, mixing at 75 °C). The contributions of carbons C1 from the glucosyl units of amylose have been enlarged on the right. The gray bars highlight the two groups of C1 positions for V7 and V8 structures. The resonances indicated by * correspond to residual fractions of B-type amylose.

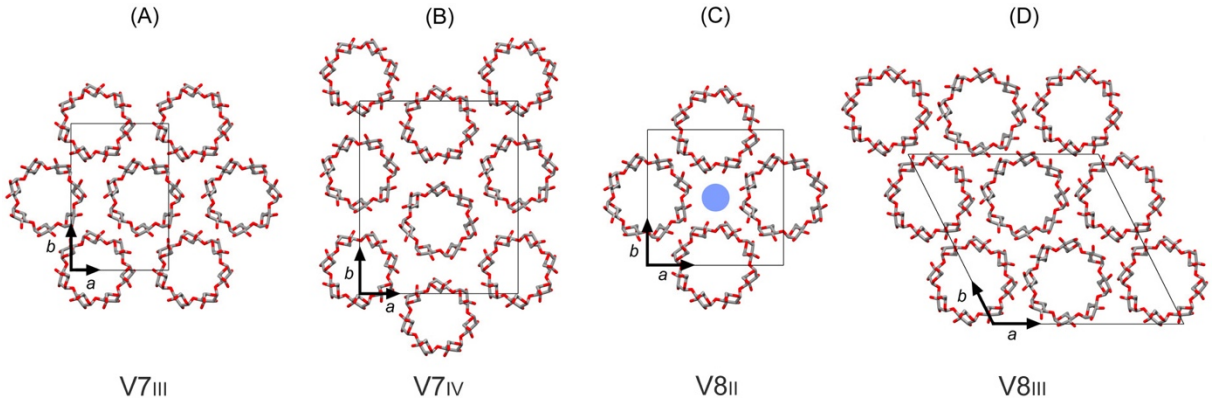

Figure 6. Geometrical molecular models of the four allomorphs of V-amylose considered in this study: (A) $V7_{III\ (NAP1)}$ based on 7-fold helices (orthorhombic unit cell with space group $P2_12_12_1$); (B) $V7_{IV\ (QN)}$ based on 7-fold helices (orthorhombic unit cell with space group $P2_12_12_1$); (C) $V8_{II\ (NAP1,\ SAL,\ QN)}$ based on 8-fold helices (tetragonal unit cell with $P4_32_12$ space group; (D) $V8_{III\ (SAL)}$ based on 8-fold helices (monoclinic unit cell with space group $P2_1$). In these base-plane projections in the (*a*,*b*) plane of the unit cells, only the amylose helices have been drawn. Hydrogen atoms have been omitted for clarity. The helices are stereoregular and the conformation of the hydroxymethyl groups has been fixed as *gg* in all cases for simplicity. In all cases, the guests can be included in the cavity of the 7- or 8-fold helices. The blue disk in (C) marks an interhelical cavity large enough to host guests. The unit cells have been superimposed on the models.

Table 2. Symmetry and unit cell parameters of V-amylose allomorphs determined from XRD data. "n.d.": not determined.

Allomorph	Ligand	Space group	Crystal system	Unit cell parameters				Number of helices per unit cell
				a (nm)	*b* (nm)	*c* (nm)	RMSE [d]	
$V7_{III}$ [a]	Napht-1-ol	$P2_12_12_1$	Orthorhombic [b]	1.663 ± 0.001	2.518 ± 0.001	0.856 ± 0.001	0.009	2
$V7_{IV}$ [a]	Quinoline	$P2_12_12_1$	Orthorhombic [b]	2.702 ± 0.001	3.291 ± 0.001	0.786 ± 0.001	0.019	4
$V8_{II}$	Napht-1-ol	$P4_32_12$	Tetragonal [b]	2.313 ± 0.006	2.313 ± 0.006	0.790 ± 0.001	0.015	2
$V8_{II}$	Salicylic acid	$P4_32_12$	Tetragonal [b]	2.306 ± 0.002	2.306 ± 0.002	0.789 ± 0.001	0.014	2
$V8_{II}$	Quinoline	$P4_32_12$	Tetragonal [b]	2.314 ± 0.003	2.314 ± 0.003	n. d.	0.021	2
$V8_{III}$ [a]	Salicylic acid	$P2_1$	Monoclinic [c]	3.245 ± 0.006	3.246 ± 0.005	0.793 ± 0.001	0.028	4

[a] new allomorph

[b] $\alpha = \beta = \gamma = 90°$

[c] $\gamma = 116.62 \pm 0.13°$

[d] root-mean-square error = $\sqrt{\sum \frac{(2\theta_{obs} - 2\theta_{cal})^2}{N_{reflections}}}$

3.4. Influence of the crystallization conditions on the mixture of allomorphs

3.4.1. $V_{napht\text{-}1\text{-}ol}$

The formation of the $V7_{III}$ and $V8_{II}$ allomorphs (**Figures 2** and **3**) depended on the DP of amylose and mixing temperature (**Table 3** and **Figure S6**). DP60 and DP80 amylose only yielded $V8_{II}$ while DP130 amylose produced a mixture of $V8_{II}$ and $V7_{III}$ in which $V8_{II}$ was the major form for all mixing temperatures. For longer amylose (DP200 and DP2500), $V8_{II}$ and $V7_{III}$ also concomitantly crystallized but the major form depended on the mixing temperature. $V8_{II}$ was the major form if the mixing temperature was 90 °C while at lower temperatures, $V7_{III}$ was the main allomorph. In previous studies, potato amylose[27,42] and DP100 synthetic amylose[32] were mixed with NAP1 at 95 °C. All resulting V_{NAP1} crystals corresponded to the $V8_{II}$ allomorph, which is consistent with our observations.

Previous studies have shown that a minimum DP was required for the formation of crystalline V-amylose (about DP 20-40).[62,63] However, this is the first time that a polymorphism that depends on the DP of amylose (both helical conformation and molecular packing in the case of V_{NAP1}) is reported. The reason for this effect of DP of amylose is still unclear. Besides, our results show that while the crystallization of V_{NAP1} occurred on cooling down to room temperature, the helical conformation and crystal structure depended on the mixing temperature. As previously mentioned by Yamashita et al.,[27] the dependence of the crystal structure on the mixing temperature rather than the incubation temperature suggests that the association of the random-coil amylose chains with NAP1 into helical complexes occurs at high temperature. The helical conformation of amylose would be decided in this critical step and would not vary upon cooling and crystallization. Previous studies also showed that a high mixing temperature was critical for the formation of crystalline V-amylose[24] and that the helical conformation depended on this temperature.[24,31]

Table 3. Allomorph of the V_{NAP1} crystals as a function of the degree of polymerization of amylose ($\overline{DP_w}$) and temperature at which napht-1-ol was added to the hot amylose solution (mixing time: 30 min). The crystals were formed upon cooling down to room temperature. For mixtures, the major and minor allomorphs are indicated.

$\overline{DP_w}$	Mixing temperature (°C)		
	60	75	90
60 and 80	$V8_{II}$	$V8_{II}$	$V8_{II}$
130	$V8_{II} > V7_{III}$	$V8_{II} > V7_{III}$	$V8_{II} > V7_{III}$
200 and 2500	$V7_{III} > V8_{II}$	$V7_{III} > V8_{II}$	$V8_{II} > V7_{III}$

3.4.2. $V_{salicylic\ acid}$

The crystallization of amylose with different DPs was conducted in dilute solution at different incubation temperatures. Two crystalline allomorphs were identified, namely and $V8_{II}$ and $V8_{III}$ (**Figures 2** and **3**). Kuge and Takeo previously reported that SAL did not form complexes with amylose in solution.[64] Later, Oguchi et al. prepared complexes with SAL using the sealed-heating method and obtained two crystal types that, according to the authors, would contain 7- and 8-fold amylose helices, respectively.[45] The V7 complex gave a powder XRD profile that is similar to that of the dry form of $V7_I$, *i.e.* $V7_a$, while the V8 complex yielded an XRD profile similar to that of $V8_{III}$.[45] Uchino et al.[46] and Guo et al.[47] also prepared V_{SAL} complexes using the sealed-heating method but they obtained a crystalline powder with a $V8_I$ structure.[47] Therefore, the present article is the first report on lamellar crystals of V_{SAL} prepared by crystallization from dilute solutions. In addition, while our results showed that V_{SAL} exhibits polymorphism, no V7 complex was identified. Although the selected crystallization conditions might have not favored the formation of 7-fold helices hosting SAL molecules, the occurrence of a V7 structure for V_{SAL} under different crystallization conditions cannot be excluded.

Table 4. Allomorph of the V_{SAL} crystals as a function of the average degree of polymerization ($\overline{DP_w}$) of amylose and incubation temperature. "-" means that no crystallization was observed after one week and the solution remained clear. For mixtures, the major and minor allomorphs are indicated.

$\overline{DP_w}$	Incubation temperature (°C)			
	25	40	60	75
60	$V8_{II}$	$V8_{II}$	-	-
130	$V8_{II}$	$V8_{III}$ > $V8_{II}$	$V8_{III}$	-
200	$V8_{III}$ > $V8_{II}$	$V8_{III}$ > $V8_{II}$	$V8_{III}$	-
2500	$V8_{III}$ > $V8_{II}$	$V8_{III}$ > $V8_{II}$	$V8_{III}$	$V8_{III}$

Table 4 and **Figure S7** summarize the allomorphic type of V_{SAL} as a function of the crystallization conditions. $V8_{III}$ was favored with the longer amylose chains and a higher crystallization temperature. In terms of packing arrangement of amylose helices, $V8_{III}$ is more compact than $V8_{II}$. Therefore, the crystallization behavior of V_{SAL} also supports the fact that higher crystallization temperatures favor more compact structures.[24] Moreover, V_{SAL} behaved like V_{NAP1} regarding the preferred formation of the $V8_{II}$ allomorph with shorter amylose chains, although both V_{SAL} allomorphs consisted of 8-fold helices while those of V_{NAP1} had different helical conformations (7- and 8-fold).

3.4.3. $V_{quinoline}$

The V_{QN} complexes were prepared using different fractions of amylose at different temperatures and solvent composition (water of DMSO / water mixtures). The crystallization always resulted in a mixture of $V7_{IV}$ and $V8_{II}$ allomorphs (**Figures 2** and **3**) but their proportion depended on the crystallization conditions (Table 5 and Figure S8). Unlike for V_{NAP1}, the crystal structure of V_{QN} did not depend on the DP of amylose which only affected the morphology of the crystals (**Figure 2E,F**). In contrast, the DMSO concentration and incubation temperature were decisive in the formation of the different allomorphs. $V8_{II}$ was generally preferred at higher concentrations of DMSO and higher crystallization temperatures. As shown in Table 5 and Figure S8, the crystallization at 25 °C or in the presence of ≤ 10 vol% DMSO mainly resulted in the formation of $V7_{IV}$ while $V8_{II}$ was the major form only in the presence of ≥ 15 vol% DMSO at 40–50 °C. Helbert previously prepared V_{QN} crystals by slowly cooling down the crystallization mixture from 90 °C to room temperature and noted that the presence of 15 vol% DMSO resulted in the formation $V8_{II}$, while $V6_{I}$ formed in the absence of DMSO.[42] This work did not clearly mention on which data the identification was based (morphology or ED / XRD diffraction data). It is possible that the $V7_{IV}$ crystals were incorrectly identified as $V6_{I}$ since their hexagonal-like shape was very similar.[17] DMSO would increase the solubility of both amylose and the complexing agent, and thus increase the concentration of complexing agent in solution. In addition, DMSO is known to affect the conformation of amylose in solution.[65–68] The observed polymorphism would thus be explained by the effect of the solvent composition on the crystal structure. Considering that DMSO has been used in many studies to easily solubilize amylose without resorting to a high-temperature heating, the role of DMSO in the crystallization of V-type complexes certainly needs clarification.

Table 5. Allomorph of the V_{QN} crystals prepared with DP2500 amylose at different incubation temperatures and DMSO concentrations. "-" means that no crystallization was observed after one week and the solution remained clear. For mixtures, the major and minor allomorphs are indicated.

DMSO (vol%)	Incubation temperature (°C)			
	25	40	50	60
0	$V7_{IV}$ >> $V8_{II}$	$V7_{IV}$ >> $V8_{II}$	-	-
10	$V7_{IV}$ >> $V8_{II}$	$V7_{IV}$ >> $V8_{II}$	-	-
15	$V7_{IV}$ > $V8_{II}$	$V8_{II}$ > $V7_{IV}$	$V8_{II}$ > $V7_{IV}$	-
25	$V7_{IV}$ > $V8_{II}$	$V8_{II}$ > $V7_{IV}$	$V8_{II}$ > $V7_{IV}$	-
30	$V7_{IV}$ > $V8_{II}$	$V8_{II}$ > $V7_{IV}$	$V8_{II}$ > $V7_{IV}$	-

4. CONCLUSION

Our results confirmed what was previously observed for V-amylose complexes with linear fatty acids,[24] aliphatic diols[31] and some bicyclic compounds:[41] some complexing agents can promote the formation of different amylose single helices (in the present case, 7- and 8-fold helices) and allomorphs, depending on specific molecular or crystallization parameters. For NAP1, the crystal structure depended on the DP of amylose and mixing temperature while for SAL, it was the DP of amylose and incubation temperature, and for QN, the concentration of added DMSO and incubation temperature. Work is in progress to identify the origin of this polymorphism (in helicity and helix distribution) for a given complexing agent in terms of solubility of amylose and guests.

By combining crystallography and spectroscopy analyses, three V-amylose allomorphs have been identified for the first time, increasing the number of known V-amylose crystal forms. So far, each of these new allomorphs has been identified for only one type of guest. Geometrical models have been proposed based on crystal morphology and symmetry considerations. In all V-amylose models, left-handed helices are arranged as antiparallel pairs, consistent with the concept of chain-folding. For $V7_{III}$, $V7_{IV}$ and $V8_{III}$, the proposed arrangements of amylose helices are compact and the complexing agents would only be located inside the helices. In contrast, there is more interstitial space in $V8_{II}$ to accommodate guest molecules, which is also the case for $V7_{II}$.[33,35]

Despite their close-packing, the helix organization in $V7_{III}$ and $V7_{IV}$ slightly deviates from the pseudo-hexagonal structure that was reported for $V7_I$ (**Figure S9**),[24,41] as is also the case for $V8_{III}$ compared to $V8_I$. The origin of these deviations cannot be identified from the tentative geometrical models drawn using stereoregular helices. Except in the case of $V8_{II}$, the interhelical spaces in all other allomorphs are too small to accommodate guests apart from water molecules. The helices possibly adopt a more elliptical cross-section due to the anisometry of the ligands. Further modeling work combining packing energy analyses and structural refinements against diffraction intensities, like the approach used by Nishiyama et al.[35] and Le et al.[38] to solve the structure of $V_{propan\text{-}2\text{-}ol}$ and $V_{butan\text{-}1\text{-}ol}$ complexes, respectively, will be carried out to confirm the helicity and conformation of amylose, as well as the helix distribution in the new allomorphs.

Over the course of their processing for food applications, starch matrices, and more particularly their amylose fraction, are likely to interact with various ingredients and additives. Depending on the nature of these molecules and the processing parameters (concentration, water content, temperature), the formation of crystalline V-type complexes may thus occur and impact specific properties of the products such as their texture, susceptibility to pH conditions,

or enzymatic resistance. In the health industry, for instance, in nutraceutical or vectorization applications, amylose can be used to entrap weakly soluble guests whose release can be modulated in controlled conditions. Therefore, the unambiguous identification of the structural signatures of each V-type allomorph and the determination of molecular models from crystallographic data are important to understand the host-guest interaction. In this work, we have described three new members of the rich V-amylose family but other allomorphs will likely be identified as more guests are tested and crystallization conditions explored.

ACKNOWLEDGMENT

We thank LabEx ARCANE and CBH-EUR-GS (grant #ANR-17-EURE-0003) for funding the PhD thesis of C.A.K.L, the Glyco@Alps program (grant #ANR-15-IDEX-02), the NanoBio-ICMG Platform (UAR 2607, Grenoble) for granting access to the electron microscopy and NMR facilities, and Henri Chanzy (CERMAV) for stimulating discussions and critical reading of the manuscript. We acknowledge the European Synchrotron Radiation Facility for providing beamtime. The WOS detector on the BM02 beamline was funded by Agence Nationale de la Recherche (grant #ANR-11-EQPX-0010). CERMAV and DPM are part of Institut Carnot PolyNat (grant #ANR-11-CARN-030-01).

REFERENCES

(1) Buléon, A.; Veronese, G.; Putaux, J.-L. Self-association and crystallization of amylose. *Aust. J. Chem.* **2007**, *60*, 706–718. https://doi.org/10.1071/CH07168

(2) Potocki de Montalk, G.; Remaud-Siméon, M.; Willemot, R. M.; Sarçabal, P.; Planchot, V.; Monsan, P. Amylosucrase from *Neisseria polysaccharea*: novel catalytic properties. *FEBS Lett.* **2000**, *471*, 219–223. https://doi.org/10.1016/S0014-5793(00)01406-X

(3) Ohdan K.; Fujii, K.; Yanase, M.; Takaha, T.; Kuriki, T. Enzymatic synthesis of amylose. *Biocatal. Biotransform.* **2006**, *24*, 77–81. https://doi.org/10.1080/10242420600598152

(4) Obiro, W. C.; Ray, S. S.; Emmambux, M. N. V-amylose structural characteristics, methods of preparation, significance, and potential applications. *Food Rev. Int.* **2012***, 28,* 412–438. https://doi.org/10.1080/87559129.2012.660718

(5) Putseys, J. A.; Lamberts, L.; Delcour, J. A. Amylose-inclusion complexes: Formation, identity and physico-chemical properties. *J. Cereal Sci.* **2010**, *51*, 238–247. https://doi.org/10.1016/j.jcs.2010.01.011

(6) Tan, L.; Kong, L. Starch-guest inclusion complexes: Formation, structure, and enzymatic digestion. *Crit. Rev. Food Sci. Nutr.* **2020**, *60*, 780–790. https://doi.org/10.1080/10408398.2018.1550739

(7) Tomasik, P.; Schilling, C. H. Complexes of starch with organic guests. *Adv. Carbohydr. Chem. Biochem.* **1998**, *53*, 345–426.

(8) Kong, L.; Perez-Santos, D. M.; Ziegler, G. R. Effect of guest structure on amylose-guest inclusion complexation. *Food Hydrocoll.* **2019**, *97*, 105188. https://doi.org/10.1016/j.foodhyd.2019.105188

(9) Ades, H.; Kesselman, E.; Ungar, Y.; Shimoni, E. Complexation with starch for encapsulation and controlled release of menthone and menthol. *LWT - Food Sci. Technol.* **2012**, *45*, 277–288. https://doi.org/10.1016/j.lwt.2011.08.008

(10) Carbinatto, F. M.; Ribeiro, T. S.; Colnago, L. A.; Evangelista, R. C.; Cury, B. S. F. Preparation and characterization of amylose inclusion complexes for drug delivery applications. *J. Pharm. Sci.* **2016**, *105*, 231–241. https://doi.org/10.1002/jps.24702

(11) Conde-Petit, B.; Escher, F.; Nuessli, J. Structural features of starch-flavor complexation in food model systems. *Trends Food Sci. Technol.* **2006**, *17*, 227–235. https://doi.org/10.1016/j.tifs.2005.11.007

(12) Di Marco, A. E.; Ixtaina, V. Y.; Tomás, M. C. Analytical and technological aspects of amylose inclusion complexes for potential applications in functional foods. *Food Biosci.* **2022**, *47*, 101625. https://doi.org/10.1016/j.fbio.2022.101625

(13) Kumar, K.; Loos, K. Deciphering structures of inclusion complexes of amylose with natural phenolic amphiphiles. *ACS Omega* **2019**, *4*, 17807–178013. https://doi.org/10.1021/acsomega.9b02388

(14) Lay Ma, U. V.; Floros, J. D.; Ziegler, G. R. Formation of inclusion complexes of starch with fatty acid esters of bioactive compounds. *Carbohydr. Polym.* **2011**, *83*, 1869–1878. https://doi.org/10.1016/j.carbpol.2010.10.055

(15) Panyoo, A. E., Emmambux, M. N. Amylose–lipid complex production and potential health benefits: A mini-review. *Starch* **2017**, *69*, 1–7. https://doi.org/10.1002/star.201600203

(16) Zhu, F. Encapsulation and delivery of food ingredients using starch-based systems. *Food Chem.* **2017**, *229*, 542–552. https://doi.org/10.1016/j.foodchem.2017.02.101

(17) Brisson, J.; Chanzy, H.; Winter, W. T. The crystal and molecular structure of V_H amylose by electron diffraction analysis. *Int. J. Biol. Macromol.* **1991**, *13*, 31–39. https://doi.org/10.1016/0141-8130(91)90007-H

(18) Buléon, A.; Delage, M.-M.; Brisson, J.; Chanzy, H. Single crystals of V amylose complexed with isopropanol and acetone. *Int. J. Biol. Macromol.* **1990**, *12*, 25–33. https://doi.org/10.1016/0141-8130(90)90078-O

(19) Yamashita, Y.-H.; Ryugo, J.; Monobe, K. An electron microscopic study on crystals of amylose V complexes. *J. Electron Microsc.* **1973**, *22*, 19–26. https://doi.org/10.1093/oxfordjournals.jmicro.a049858

(20) Manley, R. St. J. Chain folding in amylose crystals. *J. Polym. Sci. Part A* **1964**, *2*, 4503–4515.

(21) Yamashita, Y. Physicochemical study on crystalline texture of starch. II. The fold structure of amylose helices in single crystals. *Kobunshi Kagaku* **1964**, *21*, 103–108.

(22) Jacob, J.; Geßler, K.; Hoffmann, D.; Sanbe, H.; Koizumi, K.; Smith, S. M.; Takaha, T.; Saenger ,W. Band-flip and kink as novel structural motifs in α-(1→4)-D-glucose oligosaccharides. Crystal structures of cyclodeca- and cyclotetradecaamylose. *Carbohydr. Res.* **1999**, *322*, 228–246. https://doi.org/10.1016/S0008-6215(99)00216-5

(23) Biais, B.; Le Bail, P.; Robert, P.; Pontoire, B.; Buléon, A. Structural and stoichiometric studies of complexes between aroma compounds and amylose. Polymorphic transitions and quantification in amorphous and crystalline areas. *Carbohydr. Polym.* **2006,** *66*, 306–315. https://doi.org/10.1016/j.carbpol.2006.03.019

(24) Le, C. A. K.; Choisnard, L.; Wouessidjewe, D.; Putaux, J.-L. Polymorphism of crystalline complexes of amylose with fatty acids. *Int. J. Biol. Macromol.* **2018**, *119*, 555–564. https://doi.org/10.1016/j.ijbiomac.2018.07.163

(25) Yamashita, Y. Single crystals of amylose V complexes. *J. Polym. Sci. A* **1965**, *3*, 3251–3260. https://doi.org/10.1002/pol.1965.100030919

(26) Yamashita, Y.; Hirai, N. Single crystals of amylose V complexes. II. Crystals with 7_1 helical configuration. *J. Polym. Sci.Part A-2: Polym. Phys.* **1966**, *4*, 161–171. https://doi.org/10.1002/pol.1966.160040201

(27) Yamashita, Y.; K. Monobe, Single crystals of amylose V complexes. III. Crystals with 8_1 helical configuration. *J. Polym. Sci.* A2 **1971**, *9*, 1471–1481. https://doi.org/10.1002/pol.1971.160090807

(28) Zobel, H. F.; French, A. D.; Hinkle, M. E. X-ray diffraction of oriented amylose fibers. II. Structure of V amyloses. *Biopolymers* **1967**, *5*, 837–845. https://doi.org/10.1002/bip.1967.360050906

(29) Rappenecker, G.; Zugenmaier, P. Detailed refinement of the crystal structure of Vh-amylose. *Carbohydr. Res.* **1981**, *89*, 11–19. https://doi.org/10.1016/S0008-6215(00)85225-8

(30) Helbert, W.; Chanzy, H. Single crystals of V-amylose complexed with n-butanol or n-pentanol: structural features and properties. *Int. J. Biol. Macromol.* **1994**, *16*, 207–213. https://doi.org/10.1016/0141-8130(94)90052-3

(31) Le, C. A. K.; Choisnard, L.; Wouessidjewe, D.; Putaux, J.-L. Polymorphism of V-amylose co-crystallized with aliphatic diols. *Polymer* **2021**, *213*, 123302. https://doi.org/j.polymer.2020.123302

(32) Cardoso, M. B.; Putaux, J.-L.; Nishiyama, Y.; Helbert, W.; Hÿtch, M.; Silveira, N. P.; Chanzy, H. Single crystals of V-amylose complexed with α-naphthol. *Biomacromolecules* **2007**, *8*, 1319–1326. https://doi.org/10.1021/bm0611174

(33) Le, C. A. K.; Ogawa, Y.; Dubreuil, F.; Grimaud, F.; Mazeau, K.; Ziegler, G. R.; Tanwar, S.; Nishiyama, Y.; Potocki-Véronèse, G.; Choisnard, L.; Wouessidjewe, D.; Putaux, J.-L. Crystal and molecular structure of V-amylose complexed with ibuprofen. *Carbohydr. Polym.* **2021**, *261*, 117885. https://doi.org/10.1016/j.carbpol.2021.117885

(34) Lourdin, D.; Putaux, J.-L.; Potocki-Veronese, G.; Chevigny, C.; Rolland-Sabaté, A.; Buléon, A. Crystalline structure in starch, in Y. Nakamura (ed.), Starch - Metabolism and Structure, Springer Japan, **2015**, pp. 61–90.

(35) Nishiyama, Y.; Mazeau, K.; Morin, M.; Cardoso, M. B.; Chanzy, H.; Putaux, J.-L. Molecular and crystal structure of 7-fold V-amylose complexed with 2-propanol. *Macromolecules* **2010**, *43*, 8628–8636. https://doi.org/10.1021/ma101794w

(36) Valetta, R. M.; Germino, F. J.; Lang, R. E.; Moshy, R. J. Amylose "V" complexes: low molecular weight primary alcohols, *J. Polymer. Sci. A* **1964**, *2*, 1085–1094. https://doi.org/10.1002/pol.1964.100020306

(37) Godet, M. C.; Tran, V.; Delage, M.-M.; Buléon, A. Molecular modelling of the specific interactions involved in the amylose complexation by fatty acids. *Int. J. Biol. Macromol.* **1993**, *15*, 11–16. https://doi.org/10.1016/S0141-8130(05)80082-0

(38) Le, C. A. K.; Mazeau, K.; Nishiyama, Y.; Ogawa, Y.; Choisnard, L.; Wouessidjewe, D.; J.-L. Putaux. Crystal and molecular structure of V-amylose complexed with butan-1-ol. *Polymer* **2022**, *243*, 124651. https://doi.org/10.1016/j.polymer.2022.124651

(39) Winter, W. T.; Sarko, A. Crystal and molecular structure of the amylose–DMSO complex. *Biopolymers* **1974**, *13*, 1461–1482. https://doi.org/10.1002/bip.1974.360130716

(40) Hulleman, S.; Helbert, W.; Chanzy, H. Single crystals of V amylose complexed with glycerol. *Int. J. Biol. Macromol.* **1996**, *18*, 115–122. https://doi.org/10.1016/0141-8130(95)01069-6

(41) Le, C. A. K.; Choisnard, L.; Wouessidjewe, D.; Putaux, J.-L. Single crystals of V-amylose complexed with bicyclic organic compounds. *Macromol. Symp.* **2019**, *386*, 190007. https://doi.org/10.1002/masy.2019000007

(42) Helbert, W. Données sur la structure du grain d'amidon et des produits de recristallisation de l'amylose, Doctoral dissertation, **1994**, Université Joseph Fourier, France

(43) Nuessli, J.; Putaux, J.-L.; Le Bail, P.; Buléon, A. Crystal structure of amylose complexes with small ligands. *Int. J. Biol. Macromol.* **2003**, *33*, 227–234. https://doi.org/10.1016/j.ijbiomac.2003.08.009

(44) Putaux, J.-L.; Cardoso, M. B.; Morin, M.; Hu, Y.; Dupeyre, D. Single crystals of V-amylose inclusion complexes. *Macromol. Symp.* **2008**, *273*, 1–8. https://doi.org/10.1002/masy.200851301

(45) Oguchi, T.; Yamasato, H.; Limmatvapirat, S.; Yonemochi, E.; Yamamoto, K. Structural change and complexation of strictly linear amylose induced by sealed-heating with salicylic acid. *J. Chem. Soc. Faraday Trans.* **1998**, *94*, 923–927. https://doi.org/10.1039/A707848J

(46) Ushino, T.; Tozuka, Y.; Oguchi, T.; Yamamoto, K. Inclusion compound formation of amylose by sealed-heating with salicylic acid analogues. *J. Inclusion Phenom. Macrocyclic Chem.* **2002**, *43*, 31–36. https://doi.org/10.1023/A:1020418005040

(47) Guo, J.; Ziegler, G. R.; Kong, L. Polymorphic transitions of V-type amylose upon hydration and dehydration. *Food Hydrocoll.* **2022**, *125*, 107372. https://doi.org/10.1016/j.foodhyd.2021.107372

(48) Potocki-Veronese, G.; Putaux, J.-L.; Dupeyre, D.; Albenne, C.; Remaud-Simeon, M.; Monsan, P.; Buléon A. Amylose synthesized in vitro by amylosucrase: Morphology, structure, and properties. *Biomacromolecules* **2005**, *6*, 1000–1011. https://doi.org/10.1021/bm049326g

(49) MarvinSketch, https://chemaxon.com/products/marvin

(50) Laugier, J.; Bochu, B. LMGP-Suite: Suite of programs for the interpretation of X-ray experiments. http://ccp14.cryst.bbk.ac.uk/tutorial/lmgp/index.html

(51) Rappé, A. K.; Casewit, C. J.; Colwell, K.; Goddard, W.A. III; Skiff, W. M. UFF, a full periodic table force field for molecular mechanics and molecular dynamics simulations. *J. Am. Chem. Soc.* **1992***, 114*, 10024–10035. https://doi.org/10.1021/ja00051a040

(52) Materials Studio 5.5. Accelrys Inc., San Diego, CA, https://www.3dsbiovia.com/portfolio/materials-studio.html

(53) Macrae, C. F.; Bruno, I. J.; Chisholm, J. A.; Edgington, P. R.; McCabe, P.; Pidcock, E.; Rodriguez-Monge, L.; Taylor, R.; van de Streek, J.; Wood, P. A. Mercury CSD 2.0 - New features for the visualisation and investigation of crystal structures. *J. Appl. Cryst.* **2008**, *41*, 466–470. https://doi.org/10.1107/S0021889807067908

(54) Putaux, J.-L.; Nishiyama, Y.; Mazeau, K.; Morin, M.; Cardoso, M. B.; Chanzy, H. Helical conformation in crystalline inclusion complexes of V-amylose: A historical perspective. *Macromol. Symp.* **2011**, *303*, 1–9. https://doi.org/10.1002/masy.201150501

(55) Zaslow, B. Characterization of a second helical amylose modification. *Biopolymers* **1963**, *1*, 165–169. https://doi.org/10.1002/bip.360010206

(56) Gidley, M. J.; Bociek, S. M. Carbon-13 CP/MAS NMR studies of amylose inclusion complexes, cyclodextrins, and the amorphous phase of starch granules: relationships

between glycosidic linkage conformation and solid-state carbon-13 chemical shifts. *J. Am. Chem. Soc.* **1988**, *110*, 3820–3829. https://doi.org/10.1021/ja00220a016

(57) Veregin, R. P.; Fyfe, C. A.; Marchessault, R. H. Investigation of the crystalline "V" amylose complexes by high-resolution ^{13}C CP/MAS NMR spectroscopy. *Macromolecules* **1987**, *20*, 3007–3012. https://doi.org/10.1021/ma00178a010

(58) Le Bail, P.; Rondeau, C.; Buléon, A. Structural investigation of amylose complexes with small ligands: helical conformation, crystalline structure and thermostability. *Int. J. Biol. Macromol.* **2005**, *35*, 1–7. https://doi.org/10.1016/j.ijbiomac.2004.09.001

(59) Veregin, R. P.; Fyfe, C. A.; Marchessault, R. H.; Taylor, M. G. Correlation of 13C chemical shifts with torsional angles from high-resolution, ^{13}C-CP-MAS NMR studies of crystalline cyclomalto-oligosaccharide complexes, and their relation to the structures of the starch polymorphs. *Carbohydr. Res.* **1987**, *160*, 41–56. https://doi.org/10.1016/0008-6215(87)80302-6

(60) Gao, Q.; Zhang, B.; Qiu, L.; Fu, X.; Huang, Q. Ordered structure of starch inclusion complex with C10 aroma molecules. *Food Hydrocoll.* **2020**, *108*, 105969. https://doi.org/10.1016/j.foodhyd.2020.105969

(61) Rondeau-Mouro, C.; Le Bail, P.; Buléon A., Structural investigation of amylose complexes with small ligands: inter- or intra-helical associations? *Int. J. Biol. Macromol.* **2004**, *34*, 309–315. https://doi.org/10.1016/j.ijbiomac.2004.09.002

(62) Gelders, G. G.; Vanderstukken, T. C.; Goesaert, H.; Delcour, J. A. Amylose–lipid complexation: a new fractionation method. *Carbohydr. Polym.* **2004**, *56*, 447–458. https://doi.org/10.1016/j.carbpol.2004.03.012

(63) Godet, M. C.; Bizot, H.; Buléon, A. Crystallization of amylose-fatty acid complexes prepared with different amylose chain lengths. *Carbohydr. Polym.* **1995**, *27*, 47–52. https://doi.org/10.1016/0144-8617(95)00034-5

(64) Kuge, T.; Takeo, K. Complexes of starchy materials with organic compounds: part II. Complex formation in aqueous solution and fractionation of starch by *l*-menthone. *Agr. Biol. Chem.* **1968**, *32*, 1232–1238. https://doi.org/10.1080/00021369.1968.10859210

(65) Erlander, S. R.; Tobin, R. The stability of the helix of amylose and amylopectin in DMSO and water solutions. *Die Mackromolekulare Chemie* **1968**, *111*, 194–211. https://doi.org/10.1002/macp.1968.021110118

(66) Daugvilene, L. Y.; Gel'braikh, L. S.; Meyerson, S. I. Conformation transitions of macromolecules of structural amylose modifications. *Polym. Sci. USSR* **1980**, *22*, 1000–1004. https://10.1016/0032-3950(80)90294-4

(67) Nakanishi, Y.; Norisuye, T.; Teramoto A. Conformation of amylose in dimethyl sulfoxide. *Macromolecules* **1993**, *26*, 4220–4225. https://doi.org/10.1021/ma00068a023

(68) Cheetham, N. W. H.; Tao, L. Amylose conformational transitions in binary DMSO/water mixtures. *Carbohydr. Polym.* **1998**, *35*, 287–295. https://doi.org/10.1002/star.19970491006

Supporting Information

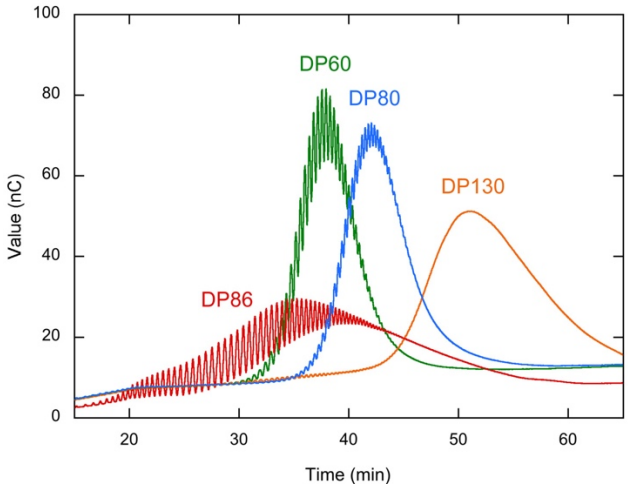

Figure S1. HPAEC chromatograms of the total amylose fraction (DP86) synthesized *in vitro* by amylosucrase and 3 fractions (DP60, DP80 and DP130) obtained by fractionation of DP86. The characteristics of each fraction are given in **Table 1** of the main manuscript. The method has been described in Le et al. (2021) and Potocki-Veronese et al. (2005).

Le, C.A.K.; Ogawa, Y.; Dubreuil, F.; Grimaud, F.; Mazeau, K.; Ziegler, G.R., Tanwar, S.; Nishiyama, Y.; Potocki-Véronèse, G.; Choisnard, L.; Wouessidjewe, D.; Putaux, J.-L. *Carbohydr. Polym.* **2021**, *261*, 117885. https://doi.org/10.1016/j.carbpol.2021.117885

Potocki-Veronese, G.; Putaux, J.-L.; Dupeyre, D.; Albenne, C.; Remaud-Simeon, M.; Monsan, P.; Buléon, A. *Biomacromolecules* **2005**, *6*, 1000–1011. https://doi.org/10.1021/bm049326g

(A) $V_{NAP1} - V8_{II}$

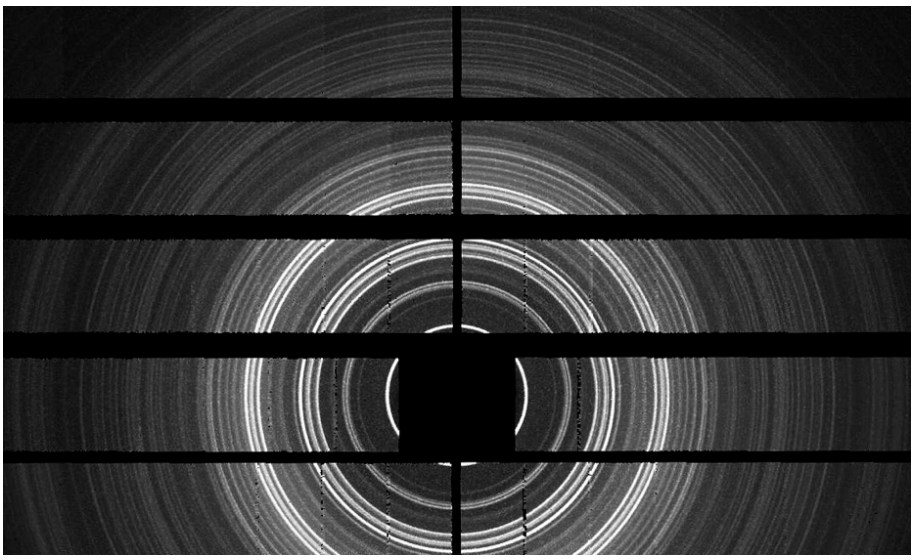

(B) $V_{SAL} - V8_{II}$

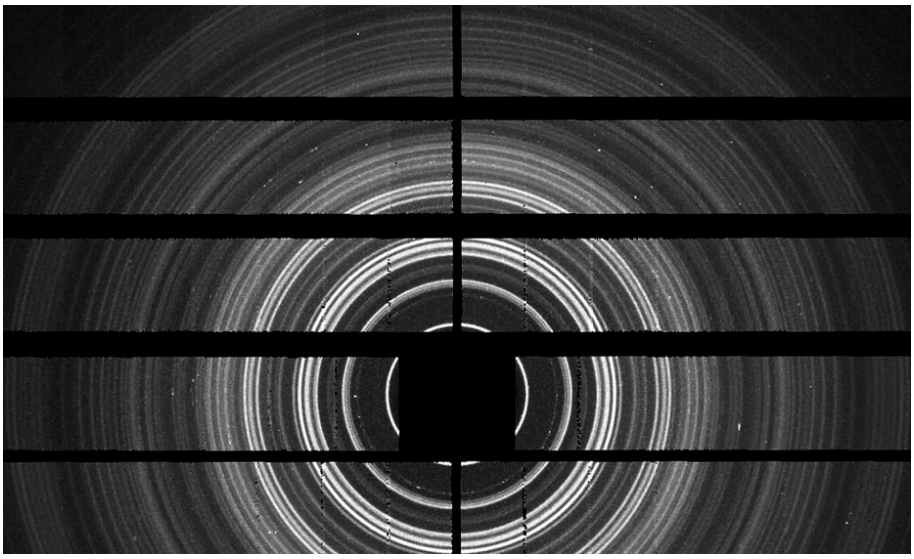

(C) $V_{NAP1} - V7_{III}$

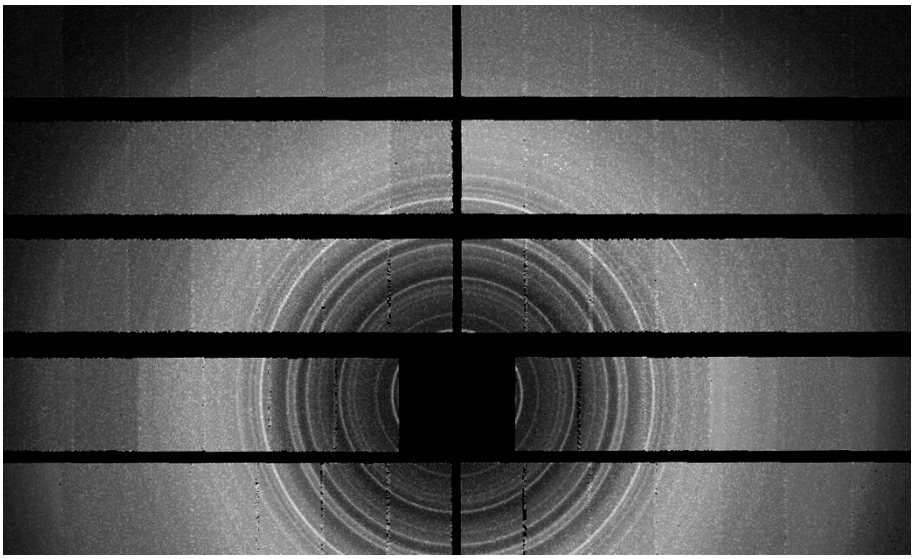

Figure S5. Continued next page.

(D) V_{SAL} – $V8_{III}$

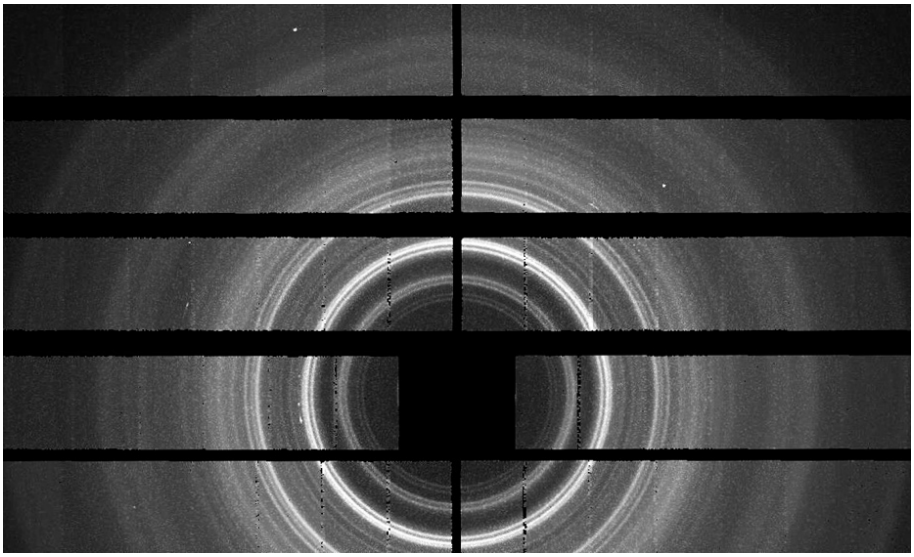

(E) V_{QN} – $V7_{IV}$

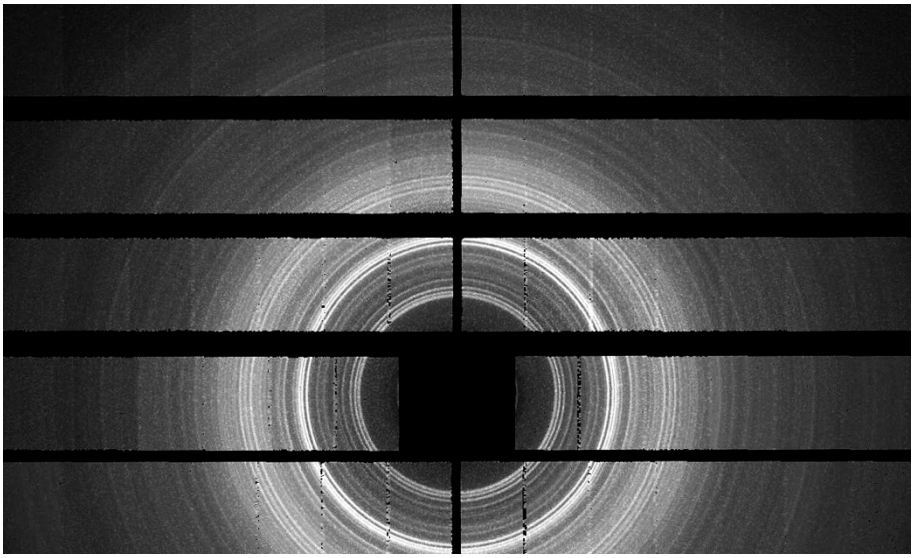

Figure S2. Synchrotron XRD patterns of hydrated samples of the V-type allomorphs prepared by crystallizing amylose in the presence of napht-1-ol (NAP1), salicylic acid (SAL) and quinoline (QN): (A) V_{NAP1} ($V8_{II}$ – DP80, mixing at 60 °C for 30 min), (B) V_{SAL} ($V8_{II}$ – DP60, 25 °C), (C) V_{NAP1} ($V7_{III}$ – DP2500, mixing at 75°C for 30 min), (D) V_{SAL} ($V8_{III}$ – DP2500, 60 °C), (E) V_{QN} ($V7_{IV}$ – DP80, no DMSO, 25 °C).

Table S1. Unit cell parameters of V-amylose allomorphs determined from XRD data collected at ESRF. "n.d.": not determined.

Allomorph	Ligand	Space group	Crystal system	Unit cell parameters				Number of helices per unit cell
				a (nm)	*b* (nm)	*c* (nm)	RMSE [d]	
$V7_{III}$ [a]	Napht-1-ol	$P2_12_12_1$	Orthorhombic [b]	1.653	2.492	n. d.	0.034	2
$V7_{IV}$ [a]	Quinoline	$P2_12_12_1$	Orthorhombic [b]	2.694	3.285	0.784	0.038	4
$V8_{II}$	Napht-1-ol	$P4_32_12$	Tetragonal [b]	2.312	2.312	0.788	0.016	2
$V8_{II}$	Salicylic acid	$P4_32_12$	Tetragonal [b]	2.294	2.294	0.787	0.028	2
$V8_{II}$	Quinoline	$P4_32_12$	Tetragonal [b]	n. d.	n. d.	n. d.	n. d.	-
$V8_{III}$ [a]	Salicylic acid	$P2_1$	Monoclinic [c]	3.242	3.248	n. d.	0.023	4

[a] new allomorph

[b] $\alpha = \beta = \gamma = 90°$

[c] $\gamma = 116.72 \pm 0.28°$

[d] root-mean-square error = $\sqrt{\sum \frac{(2\theta_{obs} - 2\theta_{cal})^2}{N_{reflections}}}$

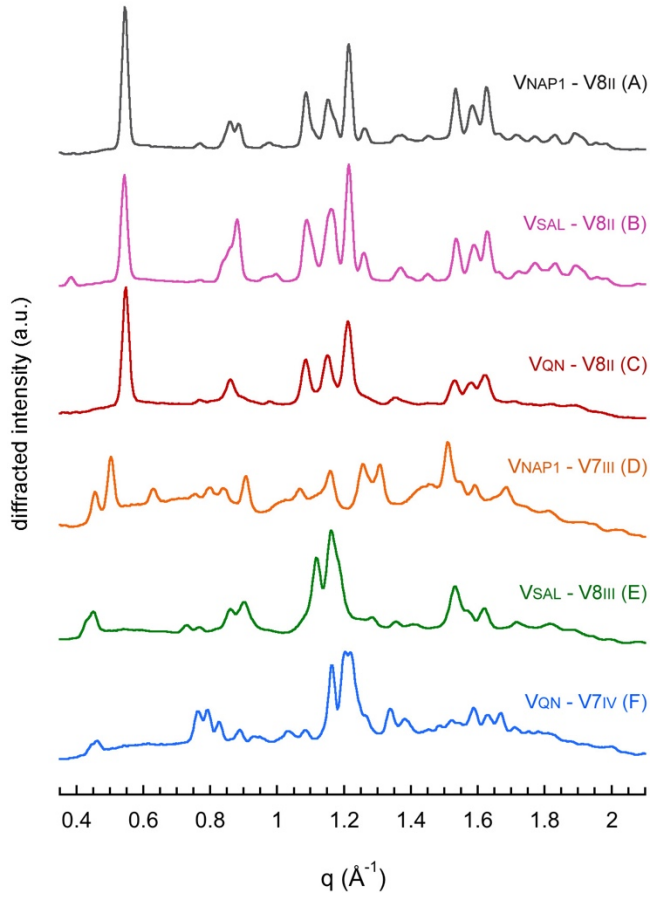

Figure S3. XRD profiles (laboratory set-up) of the V-type hydrated complexes resulting from the cocrystallization of amylose with napht-1ol (A,D), salicylic acid (B,E) and quinoline (C,F) calculated as radial averages of the 2D patterns shown in **Figures 1** and **3**: (A) V_{NAP1} ($V8_{II}$ – DP80, mixing at 60 °C for 30 min), (B) V_{SAL} ($V8_{II}$ – DP60, 25 °C), (C) V_{QN} ($V8_{II}$ – DP2500, 30 vol% DMSO, 40 °C), (D) V_{NAP1} ($V7_{III}$ – DP2500, mixing at 75 °C), (E) V_{SAL} ($V8_{III}$ – DP200, 60 °C), (F) V_{QN} ($V7_{IV}$ – DP80, no DMSO, 25 °C).

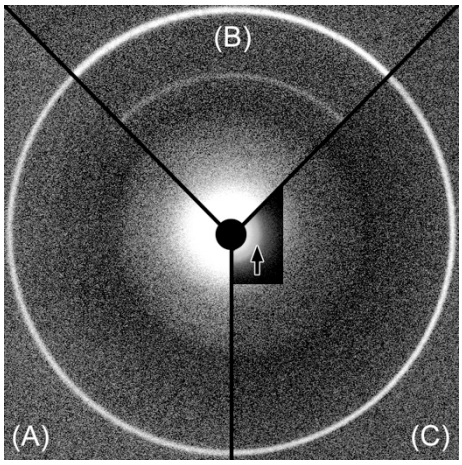

Figure S4. Comparison of the low-angle XRD powder patterns (laboratory set-up) of hydrated $V8_{II}$ complexes prepared by crystallizing amylose in the presence of napht-1-ol (A – DP130), salicylic acid (B – DP80) and quinoline (C – DP2500), focusing on a 2θ region extending to 2θ = 9°. By comparison with the patterns shown in **Figure 2C,F,I**, the sample-to-detector distance has been increased to improve the resolution at lower angle. The contrast in the central square section in C was optimized to emphasize a small-angle scattering ring (arrow) that likely corresponds to the average thickness of individual crystalline lamellae. In (A) and (B), there is no such ring and only diffuse scattering was detected.

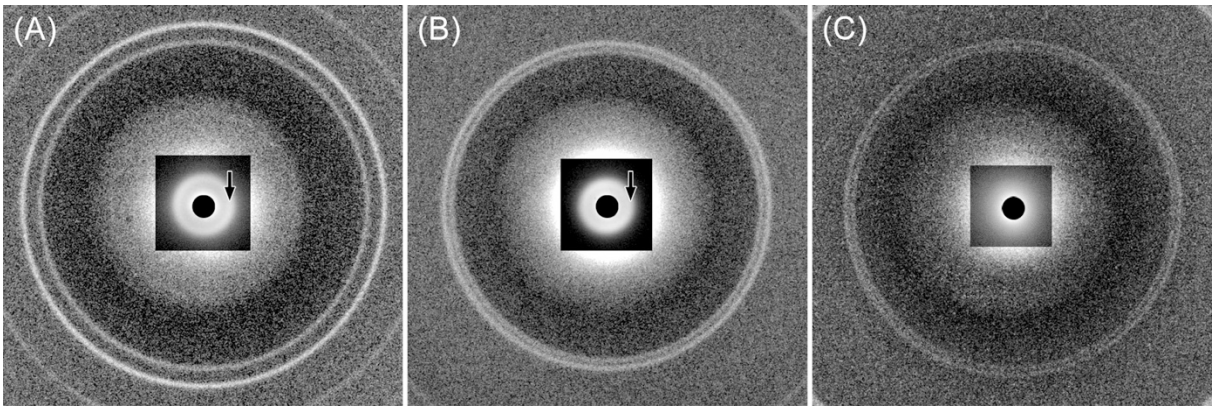

Figure S5. XRD patterns (laboratory set-up) of hydrated samples of the new V-type allomorphs prepared by crystallizing amylose in the presence of napht-1-ol (A – DP2500), salicylic acid (B – DP2500) and quinoline (C – DP80), focusing on the low-angle region extending to 2θ = 9°. By comparison with the patterns shown in **Figure 4A,F,I**, the sample-to-detector distance was increased to improve the resolution. The contrast in the central square regions was optimized to emphasize small-angle scattering rings (arrows) that likely correspond to the average thickness of individual crystalline lamellae. In (C), there is no such ring and only diffuse scattering was detected.

Table S2. Observed and calculated diffraction angles (2θ) in XRD profiles (laboratory set-up) of $V_{salicylic\ acid}$ crystals and corresponding Miller indices of the $V8_{II}$ and $V8_{III}$ allomorphs.

$V8_{II}$ [a]		
h k l	$2\theta_{obs}$ (°)	$2\theta_{cal}$ (°)
1 1 0	5.43	5.42
0 2 0	7.68	7.67
2 2 0	10.88	10.85
0 1 1	11.86	11.86
1 3 0	12.15	12.14
1 1 1	12.45	12.47
0 2 1	13.63	13.60
2 3 0	13.90	13.84
2 1 1	14.11	14.14
0 4 0	15.39	15.37
2 2 1	15.66	15.63
3 3 0	16.31	16.31
1 3 1	16.60	16.55
2 4 0	17.21	17.20
2 3 1	17.84	17.85
4 1 1	19.42	19.45
4 2 1	20.56	20.58
4 4 0	21.78	21.80
3 5 0	22.54	22.48
6 0 0	23.13	23.14
2 6 0	24.46	24.41
3 5 1	25.18	25.19
1 6 1	26.04	26.08
6 2 1	26.93	26.94

$V8_{III}$ [b]		
h k l	$2\theta_{obs}$ (°)	$2\theta_{cal}$ (°)
0 2 0	6.09	6.09
2 2 0	6.40	6.40
-2 2 0	10.37	10.38
4 2 0	10.93	10.92
4 0 0	12.23	12.20
0 2 1	12.73	12.73
4 4 0	12.81	12.82
-4 2 0	15.92	15.92
2 6 0	16.53	16.52
-1 5 0	16.87	16.87
-3 4 0	18.27	18.28
7 4 0	19.32	19.32
4 8 0	21.85	21.82
5 8 0	22.33	22.34
6 8 0	23.13	23.14
8 0 0	24.52	24.54
8 1 1	25.89	25.91
8 7 1	26.84	26.82

[a] The dataset was indexed on basis of the tetragonal unit cell: $a = b = 2.306 \pm 0.002$ nm, $c = 0.789 \pm 0.001$ nm. RMSE = $\sqrt{\sum(2\theta_{obs} - 2\theta_{cal})^2/N_{reflections}} = 0.014$.

[b] The dataset was indexed on basis of the monoclinic unit cell: $a = 3.245 \pm 0.006$ nm, $b = 3.246 \pm 0.005$ nm, $c = 0.793 \pm 0.001$ nm, $\gamma = 116.62 \pm 0.14^{o}$. RMSE = 0.028.

Table S3. Observed and calculated diffraction angles (2θ) in XRD profiles (laboratory set-up) and corresponding Miller indices of $V_{napht\text{-}1\text{-}ol}$ ($V7_{III}$) and $V_{quinoline}$ ($V7_{IV}$) crystals.

$V7_{III\ (NAP1)}$ [a]		
h k l	$2\theta_{obs}$ (°)	$2\theta_{cal}$ (°)
1 1 0	6.37	6.37
0 2 0	7.03	7.02
1 2 0	8.81	8.81
2 0 0	10.64	10.64
2 1 0	11.21	11.20
1 0 1	11.61	11.63
1 3 0	11.81	11.81
2 2 0	12.75	12.76
1 4 0	15.04	15.05
3 1 0	16.37	16.37
2 4 0	17.68	17.67
1 5 0	18.40	18.41
2 5 0	20.60	20.62
0 0 2	20.76	20.75
3 4 0	21.36	21.35
4 2 0	22.52	22.52
3 5 0	23.87	23.87

$V7_{IV\ (QN)}$ [b]		
h k l	$2\theta_{obs}$ (°)	$2\theta_{cal}$ (°)
1 2 0	6.27	6.29
2 0 0	6.55	6.54
0 4 0	10.76	10.75
3 2 0	11.20	11.20
1 0 1	11.70	11.72
2 4 0	12.59	12.60
4 0 0	13.12	13.11
4 1 0	13.41	13.38
3 4 0	14.58	14.58
2 3 1	15.34	15.34
0 6 0	16.16	16.16
1 6 0	16.49	16.49
4 4 0	16.98	16.98
5 2 0	17.27	17.27
0 5 1	17.55	17.57
1 5 1	17.95	17.88
3 6 0	18.95	18.94
5 4 0	19.65	19.66
5 2 1	20.63	20.66
0 8 0	21.59	21.60
4 5 1	21.99	21.98
6 4 0	22.52	22.51
5 6 0	23.10	23.11
7 2 0	23.68	23.68
1 3 2	24.28	24.27
3 1 2	24.83	24.85
4 8 0	25.34	25.35

[a] data indexed on the basis of the orthorhombic unit cell with $a = 1.663 \pm 0.001$ nm, $b = 2.518 \pm 0.001$ nm and $c = 0.856 \pm 0.001$ nm. RMSE = 0.009.

[b] data indexed on the basis of the orthorhombic unit cell with $a = 2.702 \pm 0.001$ nm, $b = 3.291 \pm 0.002$ nm. $c = 0.786 \pm 0.001$ nm. RMSE = 0.019.

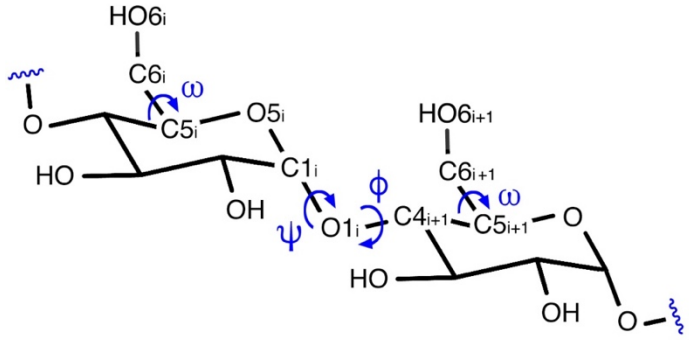

Scheme S1. Atom numbering in two contiguous glucosyl residues of the amylose chain. The ϕ and ψ torsion angles across the glycosidic bond define the relative orientation of the glucosyls. ϕ is defined by the atom sequence $O5_i$-$C1_i$-$O1_i$-$C4_{i+1}$, and ψ by $C1_i$-$O1_i$-$C4_{i+1}$-$C5_{i+1}$. The torsion ω defines the orientation of the hydroxymethyl pendant group on the pyran rings and is defined by the atom sequence $O5_i$-$C5_i$-$C6_i$-$O6_i$, and is -60, 60 and 180° for *gg*, *gt* and *tg* respectively.

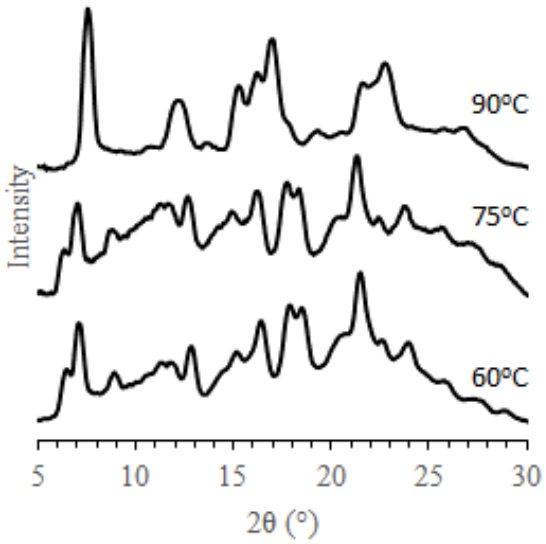

Figure S6. XRD profiles of hydrated V_{NAP1} crystals as a function of mixing temperature of DP2500 amylose solutions with an excess amount of napht-1-ol. The crystals were formed on cooling down to room temperature. The mixtures of $V7_{III}$ and $V8_{II}$ allomorphs are described in **Table 3** of the main manuscript.

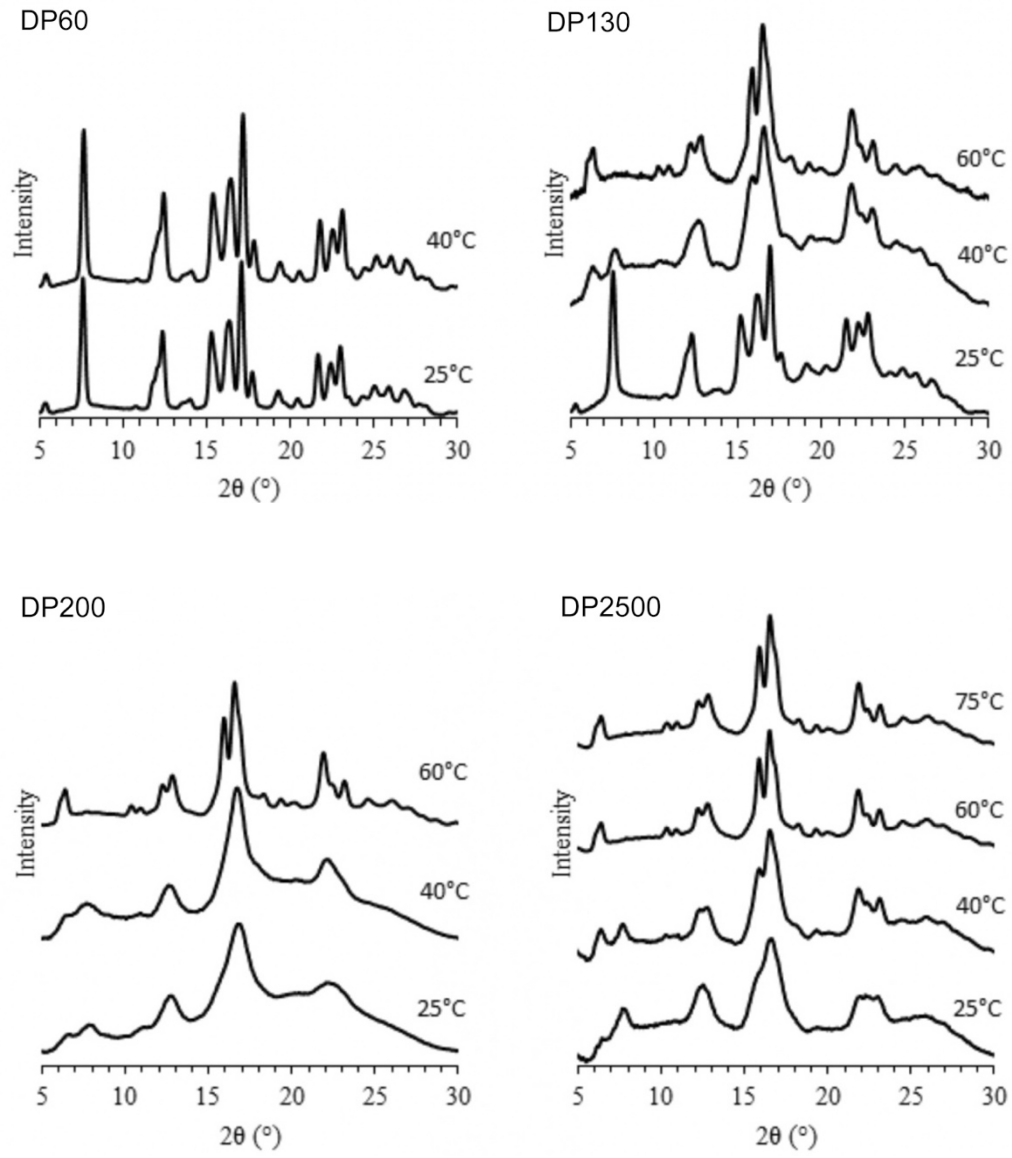

Figure S7. XRD profiles (laboratory set-up) of hydrated V_{SAL} crystals prepared from different amylose fractions in aqueous solution at different incubation temperatures. The mixtures of $V8_{II}$ and $V8_{III}$ allomorphs are described in **Table 4** of the main manuscript.

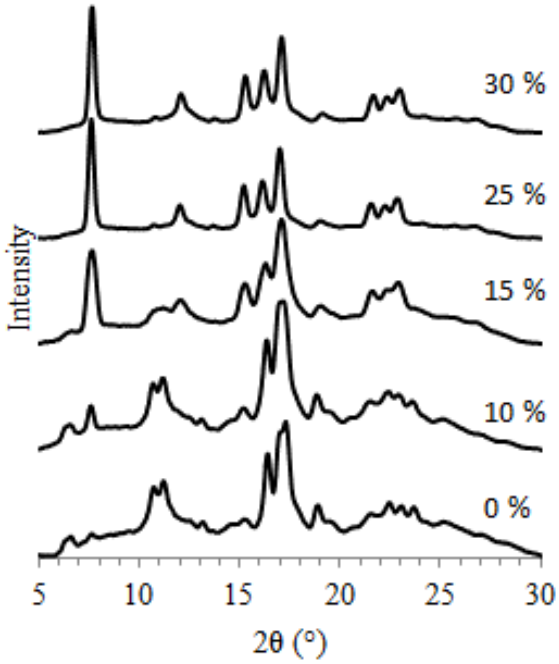

Figure S8. XRD profiles (laboratory set-up) of hydrated V_{QN} crystals as a function of DMSO concentration. The crystallization took place at 40 °C in a 0.1 wt% DP2500 amylose solution, in the presence of an excess amount of quinoline. The mixtures of $V7_{IV}$ and $V8_{II}$ allomorphs are described in **Table 5** of the main manuscript.

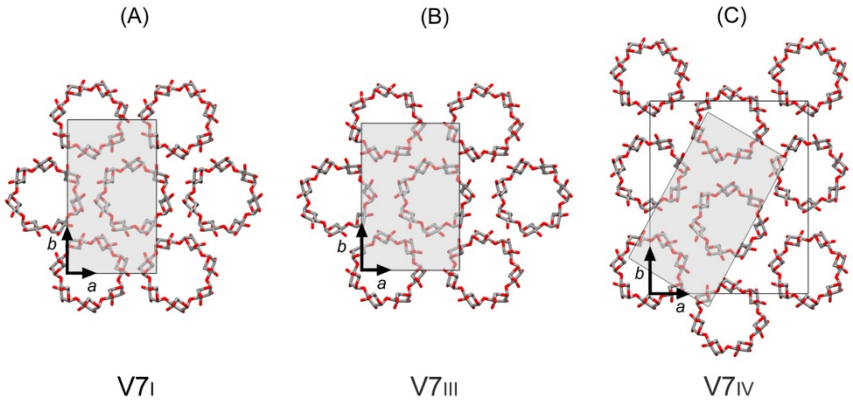

Figure S9. Surfaces in the (*a,b*) plane (in gray) of the unit cells of the $V7_I$ (A), $V7_{III}$ (B) and $V7_{IV}$ (C) allomorphs of the geometrical models shown in **Figure 6**. Only the amylose helices have been drawn. They are stereoregular and the conformation of the hydroxymethyl groups has been fixed as *gg* in all cases for simplicity. Hydrogen atoms have been omitted for clarity. The model of $V7_I$ is based on the data from Le et al. (2021) and serves as a reference for the pseudo-hexagonal compact packing of the 7-fold helices. For better comparison, the gray rectangle in $V7_{IV}$ has been drawn to consider the same helix arrangement in projection as in $V7_I$ and $V7_{III}$.

Le, C.A.K.; Choisnard, L.; Wouessidjewe, D.; Putaux, J.-L. Polymorphism of V-amylose co-crystallized with aliphatic diols. *Polymer* **2021**, *213*, 123302. https://doi.org/j.polymer.2020.123302